

Using quasar X-ray and UV flux measurements to constrain cosmological model parameters

Narayan Khadka,¹[★] and Bharat Ratra,¹[†]

¹*Department of Physics, Kansas State University, 116 Cardwell Hall, Manhattan, KS 66502, USA*

Accepted XXX. Received YYY; in original form ZZZ

ABSTRACT

Risaliti and Lusso have compiled X-ray and UV flux measurements of 1598 quasars (QSOs) in the redshift range $0.036 \leq z \leq 5.1003$, part of which, $z \sim 2.4 - 5.1$, is largely cosmologically unprobed. In this paper we use these QSO measurements, alone and in conjunction with baryon acoustic oscillation (BAO) and Hubble parameter $H(z)$ measurements, to constrain cosmological parameters in six different cosmological models, each with two different Hubble constant priors. In most of these models, given the larger uncertainties, the QSO cosmological parameter constraints are mostly consistent with those from the $H(z) + \text{BAO}$ data. A somewhat significant exception is the non-relativistic matter density parameter Ω_{m0} where the QSO data favors $\Omega_{m0} \sim 0.5 - 0.6$ in most models. Consequently in joint analyses of QSO data with $H(z) + \text{BAO}$ data the one-dimensional Ω_{m0} distributions shift slightly toward larger values. A joint analysis of the QSO + $H(z)$ + BAO data is consistent with the current standard model, spatially-flat ΛCDM , but mildly favors closed spatial hypersurfaces and dynamical dark energy. Since the higher Ω_{m0} values favored by the QSO data appear to be associated with the $z \sim 2 - 5$ part of these data, and conflict somewhat with strong indications for $\Omega_{m0} \sim 0.3$ from most $z < 2.5$ data as well as from the cosmic microwave background anisotropy data at $z \sim 1100$, in most models, the larger QSO data Ω_{m0} is possibly more indicative of an issue with the $z \sim 2 - 5$ QSO data than of an inadequacy of the standard flat ΛCDM model.

Key words: (*cosmology:*) cosmological parameters – (*cosmology:*) observations – (*cosmology:*) dark energy

1 INTRODUCTION

It is a well-established fact that the universe is now undergoing accelerated cosmological expansion. In general relativity, hypothetical dark energy is responsible for the observed acceleration of the cosmological expansion. The simplest cosmological model consistent with this accelerated expansion is the flat ΛCDM model, the current standard model (Peebles 1984). In this model the accelerated expansion is powered by the spatially homogenous cosmological constant (Λ) energy density which is constant in time. This model is consistent with many observations (Alam et al. 2017; Farooq et al. 2017; Scolnic et al. 2018; Planck Collaboration 2018) when dark energy contributes about 70% of the current cosmological energy budget, with about 25% contributed from cold dark matter (CDM), and the remaining 5% due to

baryons. The standard model assumes flat spatial hypersurfaces.

While the ΛCDM model is consistent with many observations, it is based on the assumption of a time-independent and spatially-homogeneous dark energy density that is difficult to theoretically motivate. Additionally, observations do not demand a time-independent dark energy density, and models in which the dark energy density decreases with time have been studied. In addition to the ΛCDM model, here we consider two dynamical dark energy models, the XCDM parametrization with a dynamical dark energy X -fluid and the ϕCDM model with a dynamical dark energy scalar field ϕ .

While cosmological models with vanishing spatial curvature are consistent with many observations, current observations allow a little spatial curvature.¹ So here, in addition

[★] E-mail: nkhadka@phys.ksu.edu

[†] E-mail: ratra@phys.ksu.edu

¹ Discussion of observational constraints on spatial curvature may be traced through Farooq et al. (2015), Chen et al. (2016), Yu & Wang (2016), Rana et al. (2017), Ooba et al. (2018a,b,c), DES

to flat models, we also consider non-flat models with non-zero spatial curvature energy density. In this paper we test six different cosmological models, three spatially flat and three spatially non-flat.

These cosmological models have mostly been tested with data from low redshifts $z \sim 0$ up to redshift $z \sim 2.4$ baryon acoustic oscillation (BAO) measurements, as well as with cosmic microwave background (CMB) anisotropy data at $z \sim 1100$. They are poorly tested against data in the redshift range between ~ 2.5 and ~ 1100 . To establish an accurate cosmological model and tighten cosmological parameter constraints, it is important to use additional cosmological probes, such as the quasar (QSO) flux - redshift data studied here. These QSO data probe the universe to $z \sim 5$ and are one of the few data sets that probe the $z \sim 2.5-5$ redshift range.²

In 2015 Risaliti and Lusso published a systematic study that used quasar measurements to constrain cosmological parameters. The Risaliti & Lusso (2015) quasar sample has 808 quasar measurements extending over a redshift range $0.061 \leq z \leq 6.28$ which covers a significant part of the universe. These data have been used to constrain cosmological parameters (Risaliti & Lusso 2015; López-Corredoria et al. 2016; Lazkoz et al. 2019; Khadka & Ratra 2020) and the constraints obtained are consistent with those obtained from most other cosmological probes. However, the QSO data constraints (Khadka & Ratra 2020) have larger error bars than those that result from BAO, Hubble parameter [$H(z)$], and some other data. This is because the empirical relation between the quasar's X-ray and UV luminosity, that is the basis of this method, has a large dispersion ($\delta = 0.32 \pm 0.008$). In 2019 Risaliti and Lusso enhanced these data by compiling a larger sample of quasars (Risaliti & Lusso 2019). For cosmological purposes, they selected 1598 quasars from a much larger number of sources. The dispersion of the $L_X - L_{UV}$ relation obtained from the new set of 1598 quasar measurements is smaller ($\delta = 0.23 \pm 0.004$) than that for the Risaliti & Lusso (2015) data. On the other hand, these new data give a relatively higher value of the matter density parameter in almost all models. This is one of the notable differences between the 2015 QSO and 2019 QSO data.

One major goal of our paper is to use the Risaliti & Lusso (2019) QSO data to constrain cosmological parameters in six cosmological models. Also, we study the effect of two different Hubble constant priors on the cosmological parameter constraints. Since we use a number of different cosmological models here, we are able to draw somewhat model-independent conclusions about the QSO data constraints. We find that the QSO data by themselves do not

provide restrictive constraints on cosmological parameters. However, given the larger error bars, the QSO constraints are mostly consistent with those that follow from the $H(z) +$ BAO data, and when jointly analyzed the 2019 QSO measurements slightly tighten $H(z) +$ BAO data constraints in some of the models (but less so than did the 2015 QSO data, Khadka & Ratra 2020) and, more significantly, shift the matter density parameter (Ω_{m0}) in most of the models to higher values. The QSO + $H(z) +$ BAO data are consistent with the standard flat Λ CDM cosmological model although they mildly favor closed spatial hypersurfaces over flat ones and dynamical dark energy over a cosmological constant.

In most of the models we study here, the 2019 QSO data favor $\Omega_{m0} \sim 0.5-0.6$. Risaliti & Lusso (2019) verify that the $z < 1.4$ part of the QSO data are consistent with $\Omega_{m0} \sim 0.3$, which is also favored by most data up to $z \sim 2.5$, as well as by CMB anisotropy data at $z \sim 1100$, in most cosmological models. This 2019 QSO data preference for $\Omega_{m0} \sim 0.5-0.6$ is therefore possibly more an indication of an issue with the $z \sim 2-5$ 2019 QSO data, and less an indication of the invalidity of the standard Λ CDM model (Risaliti & Lusso 2019; Lusso et al. 2019). Since the QSO data is one of the very few probes of the $z \sim 2-5$ part of the universe, it is important to resolve this issue.

Our paper is organized as follows. In Sec. 2 we describe the models that we use. In Sec. 3 we discuss the data we use to constrain cosmological parameters. In Sec. 4 we describe the techniques we use in our analyses. In Sec. 5 we compare 2019 QSO and 2015 QSO data constraints and present cosmological parameter constraints from the 2019 QSO data and the 2019 QSO + $H(z) +$ BAO data. We conclude in Sec. 6.

2 MODELS

We use one time-independent and two dynamical dark energy models to constrain cosmological parameters. We use spatially-flat and non-flat versions of each dark energy cosmological model and study a total of six cosmological models. For dark energy we use a cosmological constant Λ in the Λ CDM model, as well as an X -fluid dynamical dark energy density in the XCDM parametrization, and a scalar field ϕ dynamical dark energy density in the ϕ CDM model.

In the Λ CDM model the redshift dependence of the Hubble parameter is

$$H(z) = H_0 \sqrt{\Omega_{m0}(1+z)^3 + \Omega_{k0}(1+z)^2 + \Omega_{\Lambda}}, \quad (1)$$

where $\Omega_{m0} + \Omega_{k0} + \Omega_{\Lambda} = 1$. Here Ω_{Λ} is the dark energy density parameter and Ω_{m0} and Ω_{k0} are the current values of the non-relativistic matter and the spatial curvature energy density parameters. In the spatially-flat Λ CDM model we choose Ω_{m0} and H_0 to be the free parameters while in the spatially non-flat Λ CDM model we choose Ω_{m0} , Ω_{Λ} , and H_0 to be the free parameters.

In the XCDM parametrization the dynamical dark energy density decreases with time. In this case dark energy is modeled as a fluid with equation of state $P_X = \omega_X \rho_X$. Here P_X and ρ_X are the pressure and energy density of the X -fluid, and ω_X is the equation of state parameter whose value is negative ($\omega_X < -1/3$). In this parametrization the

Collaboration (2018a), Yu et al. (2018), Park & Ratra (2018a,b,c, 2019, 2020), Wei & Wu (2018), Xu et al. (2019), Ruan et al. (2019), Li et al. (2019), Giambó et al. (2019), Coley (2019), Eingorn et al. (2019), Jesus et al. (2019), Handley et al. (2019), Wang et al. (2019), Zhai et al. (2019), Geng et al. (2020), Kumar et al. (2020), Efstathiou & Gratton (2020), Di Valentino et al. (2020) and references therein.

² In the last decade or so, HII starburst galaxy data has reached to $z \sim 2.5$ (Siegel et al. 2005; Mania & Ratra 2012; González-Morán et al. 2019, and references therein) while gamma ray burst data reach to $z \sim 8$ (Lamb & Reichart 2000; Samushia & Ratra 2010; Demianski et al. 2019, and references therein).

Hubble parameter is

$$H(z) = H_0 \sqrt{\Omega_{m0}(1+z)^3 + \Omega_{k0}(1+z)^2 + \Omega_{X0}(1+z)^{3(1+\omega_X)}}, \quad (2)$$

where $\Omega_{m0} + \Omega_{k0} + \Omega_{X0} = 1$ and Ω_{X0} is the current value of the X -fluid energy density parameter. In the spatially-flat case we choose Ω_{m0} , ω_X , and H_0 to be the free parameters while in the non-flat case we choose Ω_{m0} , Ω_{k0} , ω_X , and H_0 to be the free parameters. In the $\omega_X = -1$ limit the Λ CDM parametrization becomes the Λ CDM model.

In the ϕ CDM model a scalar field ϕ with potential energy density $V(\phi)$ provides the dynamical dark energy density that decreases with time (Peebles & Ratra 1988; Ratra & Peebles 1988; Pavlov et al. 2013).³ A widely used $V(\phi)$ has the inverse power law form

$$V(\phi) = \frac{1}{2} \kappa m_p^2 \phi^{-\alpha}, \quad (3)$$

with m_p being the Planck mass, α a positive parameter, and

$$\kappa = \frac{8}{3} \left(\frac{\alpha + 4}{\alpha + 2} \right) \left[\frac{2}{3} \alpha (\alpha + 2) \right]^{\alpha/2}. \quad (4)$$

The equations of motion of this model are

$$\ddot{\phi} + \frac{3\dot{a}}{a} \dot{\phi} - \frac{1}{2} \alpha \kappa m_p^2 \phi^{-\alpha-1} = 0, \quad (5)$$

and

$$\left(\frac{\dot{a}}{a} \right)^2 = \frac{8\pi G}{3} (\rho_m + \rho_\phi) - \frac{k}{a^2}. \quad (6)$$

Here a is the scale factor, an overdot denotes a derivative with respect to time, k is negative, zero, and positive for open, flat, and closed spatial hypersurfaces, ρ_m is the non-relativistic matter density, and the scalar field energy density is

$$\rho_\phi = \frac{m_p^2}{32\pi} [\dot{\phi}^2 + \kappa m_p^2 \phi^{-\alpha}]. \quad (7)$$

In the ϕ CDM model the Hubble parameter is

$$H(z) = H_0 \sqrt{\Omega_{m0}(1+z)^3 + \Omega_{k0}(1+z)^2 + \Omega_\phi(z, \alpha)}, \quad (8)$$

where

$$\Omega_\phi(z, \alpha) = \frac{8\pi G \rho_\phi}{3H_0^2}, \quad (9)$$

with G being the gravitational constant and $\Omega_{m0} + \Omega_{k0} + \Omega_\phi(0, \alpha) = 1$. In the ϕ CDM model $\Omega_\phi(z, \alpha)$ has to be numerically computed. In the spatially non-flat ϕ CDM model we choose Ω_{m0} , Ω_{k0} , α , and H_0 to be the free parameters while in the spatially-flat ϕ CDM model we choose Ω_{m0} , α , and H_0 to be the free parameters. In the limit $\alpha \rightarrow 0$ the ϕ CDM model becomes the Λ CDM model.

³ For discussions of observational constraints on the ϕ CDM model see Chen & Ratra (2004), Samushia et al. (2007), Yashar et al. (2009), Samushia & Ratra (2010), Samushia et al. (2010), Chen & Ratra (2011b), Campanelli et al. (2012), Farooq & Ratra (2013), Farooq et al. (2013), Avsajanishvili et al. (2015), Sòla et al. (2017), Sòla Peracaula et al. (2018, 2019), Zhai et al. (2017), Sangwan et al. (2018), Singh et al. (2019), Mitra et al. (2019), and references therein.

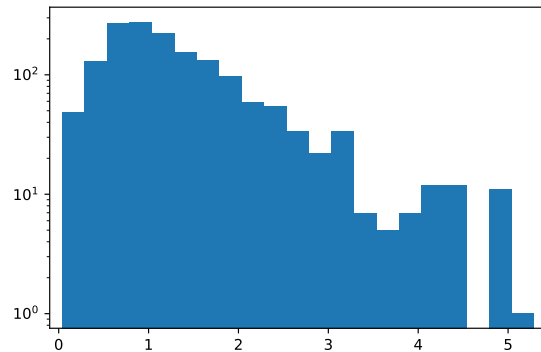


Figure 1. Redshift distribution of the Risaliti and Lusso 2019 QSO data.

3 DATA

The Risaliti & Lusso (2015) QSO compilation has 808 quasar flux-redshift measurements over a redshift range $0.061 \leq z \leq 6.28$. In this compilation most of the quasars are at high redshift, $\sim 77\%$ are at $z > 1$ and only $\sim 23\%$ are at $z < 1$. These data have a larger intrinsic dispersion ($\delta = 0.32 \pm 0.008$) in the $L_X - L_{UV}$ X-ray and UV luminosity relation which affects the error bars and so these data do not tightly constrain cosmological parameters. See Khadka & Ratra (2020) for cosmological parameter constraints obtained from the 2015 QSO data.

To improve upon their 2015 data set, in 2019 Risaliti and Lusso published a compilation of 1598 quasars, chosen for the purpose of constraining cosmological parameters from a large sample of 7,237 sources (Risaliti & Lusso 2019). A significant portion of the QSOs in this new compilation are at lower redshift ($\sim 43\%$ are at redshift $z \leq 1$), with QSOs in this new compilation distributed more uniformly over a smaller redshift range of $0.036 \leq z \leq 5.1003$ in comparison to the old data. The redshift distribution of the new quasar data is shown in Fig. 1. These QSOs have an $L_X - L_{UV}$ relation with a smaller intrinsic dispersion ($\delta = 0.23 \pm 0.004$). The main purpose of our paper is to use the 1598 QSO X-ray and UV flux measurements of Risaliti & Lusso (2019) to determine cosmological parameter constraints.⁴ We also compare the constraints from the 2019 QSO data to those that follow from the earlier Risaliti & Lusso (2015) QSO compilation.

Additionally, we compare the 2019 QSO data cosmological parameter constraints to those determined from more widely used BAO distance measurements and $H(z)$ observations. The $H(z)$ and BAO data we use consist of 31 $H(z)$ measurements over the redshift range $0.07 \leq z \leq 1.965$ and 11 BAO measurements over the redshift range $0.106 \leq z \leq 2.36$. The $H(z)$ and BAO data we use are given in Table 2 of Ryan et al. (2018) and Table 1 of Ryan et al. (2019).

⁴ For cosmological parameter constraints derived from the 2019 QSO data, see Risaliti & Lusso (2019), Lusso et al. (2019), Melia (2019), Yang et al. (2019), Velten & Gomes (2020), Wei & Melia (2020), Lindner et al. (2020), Zheng et al. (2020), and Mehrabi & Basilakos (2020).

4 METHOD

Over the last four decades it has become clear that a quasar's X-ray and UV luminosities are non-linearly correlated (Tananbaum et al. 1979; Zamorani et al. 1981; Avni & Tananbaum 1986; Steffen et al. 2006; Just et al. 2007; Young et al. 2010; Lusso et al. 2010; Grupe et al. 2010; Vagnetti et al. 2010). Risaliti & Lusso (2015) made use of this correlation to constrain cosmological model parameters, as follows. The empirical relation between the quasar's X-ray and UV luminosity is

$$\log(L_X) = \beta + \gamma \log(L_{UV}), \quad (10)$$

where $\log = \log_{10}$ and L_X and L_{UV} are the QSO X-ray and UV luminosities and β and γ are free parameters to be determined from the data.

What is directly observed are the fluxes and so we need a relation between the X-ray and UV fluxes. Expressing the luminosity in terms of the flux we obtain

$$\log(F_X) = \beta + (\gamma - 1) \log(4\pi) + \gamma \log(F_{UV}) + 2(\gamma - 1) \log(D_L), \quad (11)$$

where F_X and F_{UV} are the X-ray and UV fluxes respectively. Here $D_L(z, p)$ is the luminosity distance, which is a function of redshift and the set of cosmological model parameters, p , and is given by

$$\frac{H_0 \sqrt{|\Omega_{k0}|} D_L(z, p)}{(1+z)} = \begin{cases} \sinh[g(z)] & \text{if } \Omega_{k0} > 0, \\ g(z) & \text{if } \Omega_{k0} = 0, \\ \sin[g(z)] & \text{if } \Omega_{k0} < 0, \end{cases} \quad (12)$$

where

$$g(z) = H_0 \sqrt{|\Omega_{k0}|} \int_0^z \frac{dz'}{H(z')}, \quad (13)$$

and the Hubble parameter $H(z)$, which is a function of cosmological model parameters, is given in Sec. 2 for each of the six cosmological models we study in this paper.

To constrain cosmological parameters we compare observed X-ray fluxes to model-predicted X-ray fluxes at the same redshifts. The model-predicted X-ray flux of a QSO depends on the set of cosmological parameters, the redshift, and the observed UV flux, see eq. (11). We determine the best-fit values and uncertainty of the cosmological parameters for a given model by maximizing the likelihood function. The QSO data analysis depends on the $L_X - L_{UV}$ relation and this relation has an observed dispersion (δ). So we are required to consider a likelihood function normalization factor which is a function of δ . The likelihood function (LF) for QSO data is (Risaliti & Lusso 2015)

$$\ln(\text{LF}) = -\frac{1}{2} \sum_{i=1}^{1598} \left[\frac{[\log(F_{X,i}^{\text{obs}}) - \log(F_{X,i}^{\text{th}})]^2}{s_i^2} + \ln(2\pi s_i^2) \right], \quad (14)$$

where $\ln = \log_e$ and $s_i^2 = \sigma_i^2 + \delta^2$, and σ_i and δ are the measurement error on $F_{X,i}^{\text{obs}}$ and the global intrinsic dispersion respectively. In eq. (14) $F_{X,i}^{\text{th}}$ is the corresponding model prediction defined by eq. (11), and is a function of the observed F_{UV} and $D_L(z_i, p)$. We treat δ as a free parameter to be determined by the data, along with the other two free parameters, β and γ , which characterise the $L_X - L_{UV}$ relation in eq. (10). In Risaliti & Lusso (2019), also see Lusso et al. (2019), γ is not a free parameter, β is determined by calibrating quasar distance modulus using JLA supernovae data

over the common redshift range $z < 1.4$, and δ is a free parameter, whereas in Wei & Melia (2020) β is determined by calibrating quasar distance modulus using Hubble parameter measurements, and γ and δ are free parameters. We instead follow Khadka & Ratra (2020) and treat β , γ , and δ as free parameters to be determined, along with the cosmological parameters, from the QSO data, in each cosmological model. As a consequence, our QSO constraints are QSO-only constraints (they do not make use of the supernovae or $H(z)$ data),⁵ which makes them a little less constraining than the Risaliti & Lusso (2019) results, but allows us to compare QSO-only constraints to those from other data.

Our determination of the BAO and $H(z)$ data constraints uses the procedure outlined in Sec. 4 of Khadka & Ratra (2020).

For all parameters except H_0 , we use top hat priors, non-zero over the ranges $0 \leq \Omega_{m0} \leq 1$, $0 \leq \Omega_\Lambda \leq 1.3$, $-0.7 \leq k \leq 0.7$, $-20 \leq \omega_X \leq 5$, $0 \leq \alpha \leq 3$, $-10 \leq \ln \delta \leq 10$, $0 \leq \beta \leq 11$, and $-2 \leq \gamma \leq 2$. Here $k = -\Omega_{k0} a_0^2$ where a_0 is the current value of the scale factor. For H_0 we consider two different Gaussian priors, $H_0 = 68 \pm 2.8 \text{ km s}^{-1} \text{ Mpc}^{-1}$, from a median statistics analysis of a large compilation of H_0 measurements (Chen & Ratra 2011a),⁶ and $H_0 = 73.24 \pm 1.74 \text{ km s}^{-1} \text{ Mpc}^{-1}$, from a recent local expansion rate measurement (Riess et al. 2016).⁷

The likelihood analysis is performed using the Markov chain Monte Carlo (MCMC) method as implemented in the emcee package (Foreman-Mackey et al. 2013) in Python 3.7.

For the QSO data we use the maximum likelihood value LF_{max} to compute the minimum $\chi_{\text{min,QSO}}^2 = -2 \ln(\text{LF}_{\text{max,QSO}}) - \sum_{i=1}^{1598} \ln(2\pi(\sigma_{i,\text{QSO}}^2 + \delta_{\text{bestfit}}^2))$.⁸ The second term in the expression for $\chi_{\text{min,QSO}}^2$ is a consequence of the normalization factor in the QSO likelihood function, see eq. (14). The χ_{min}^2 for the QSO + $H(z)$ + BAO data set also accounts for the QSO normalization factor, while in the case of the $H(z)$ + BAO data set we compute the conventional minimum $\chi_{\text{min,H(z)+BAO}}^2 = -2 \ln(\text{LF}_{\text{max,H(z)+BAO}})$. In addition

⁵ As discussed below, we do use two different H_0 priors for analysing the QSO data, however the derived QSO constraints on parameters, excluding that on H_0 , are almost insensitive to the choice of H_0 prior.

⁶ This value is very consistent with those from earlier median statistics analyses (Gott et al. 2001; Chen et al. 2003), and with many recent measurements of H_0 (Chen et al. 2017; DES Collaboration 2018b; Yu et al. 2018; Gómez-Valent & Amendola 2018; Haridasu et al. 2018; Planck Collaboration 2018; Zhang 2018; Domínguez et al. 2019; Martinelli & Tutusaus 2019; Cuceu et al. 2019; Zeng & Yan 2019; SchÅneberg et al. 2019; Lin & Ishak 2019; Rameez & Sarkar 2019; Zhang & Huang 2019).

⁷ Other local expansion rate determinations result in somewhat lower H_0 values with somewhat larger error bars (Rigault et al. 2015; Zhang et al. 2017; Dhawan et al. 2017; Fernandez Arenas et al. 2018; Freedman et al. 2019, 2020).

⁸ In Khadka & Ratra (2020), the χ_{min}^2 for the QSO data was incorrectly computed using the conventional minimum $-2 \ln(\text{LF}_{\text{max}})$. This resulted in an incorrect, low, reduced χ_{min}^2 for the 2015 QSO data, < 0.6 , see Tables 1 and 2 of Khadka & Ratra (2020). Including the normalization factor in the computation of χ_{min}^2 for the 2015 QSO data, the reduced χ_{min}^2 are very close to unity in all models.

Table 1. Marginalized one-dimensional best-fit parameters with 1σ confidence intervals for all models using 2019 and 2015 QSO data for the $H_0 = 68 \pm 2.8 \text{ km s}^{-1} \text{ Mpc}^{-1}$ prior.

Data	Model	Ω_{m0}	Ω_Λ	Ω_{k0}	ω_X	α	H_0^a	δ	β	γ
2019 QSO data	Flat Λ CDM	$0.64^{+0.21}_{-0.19}$	-	-	-	-	$68.00^{+2.80}_{-2.79}$	$0.23^{+0.004}_{-0.004}$	$7.58^{+0.33}_{-0.34}$	$0.62^{+0.01}_{-0.01}$
	Non-flat Λ CDM	$0.64^{+0.20}_{-0.17}$	$0.84^{+0.23}_{-0.34}$	$-0.48^{+0.51}_{-0.43}$	-	-	$67.95^{+2.79}_{-2.76}$	$0.23^{+0.004}_{-0.004}$	$7.91^{+0.41}_{-0.41}$	$0.61^{+0.01}_{-0.01}$
	Flat XCDM	$0.28^{+0.26}_{-0.14}$	-	-	$-9.57^{+4.60}_{-6.31}$	-	$68.02^{+2.76}_{-2.79}$	$0.23^{+0.004}_{-0.004}$	$7.78^{+0.31}_{-0.32}$	$0.62^{+0.01}_{-0.01}$
	Non-flat XCDM	$0.42^{+0.26}_{-0.18}$	-	$-0.12^{+0.15}_{-0.19}$	$-5.74^{+2.97}_{-6.43}$	-	$68.01^{+2.81}_{-2.78}$	$0.23^{+0.004}_{-0.004}$	$8.01^{+0.43}_{-0.44}$	$0.61^{+0.01}_{-0.01}$
	Flat ϕ CDM	$0.61^{+0.20}_{-0.20}$	-	-	-	$1.30^{+1.11}_{-0.94}$	$68.01^{+2.78}_{-2.78}$	$0.23^{+0.004}_{-0.004}$	$7.59^{+0.33}_{-0.35}$	$0.62^{+0.01}_{-0.01}$
	Non-flat ϕ CDM	$0.57^{+0.22}_{-0.20}$	-	$-0.29^{+0.35}_{-0.27}$	-	$1.29^{+1.13}_{-0.93}$	$68.03^{+2.78}_{-2.76}$	$0.23^{+0.004}_{-0.004}$	$7.73^{+0.38}_{-0.38}$	$0.62^{+0.01}_{-0.01}$
2015 QSO data ^b	Flat Λ CDM	$0.26^{+0.17}_{-0.11}$	-	-	-	-	$68.00^{+2.8}_{-2.8}$	$0.32^{+0.008}_{-0.008}$	$8.42^{+0.57}_{-0.58}$	$0.59^{+0.02}_{-0.02}$
	Non-flat Λ CDM	$0.24^{+0.16}_{-0.17}$	$0.93^{+0.18}_{-0.39}$	$-0.17^{+0.49}_{-0.34}$	-	-	$68.00^{+2.8}_{-2.8}$	$0.32^{+0.008}_{-0.008}$	$8.62^{+0.62}_{-0.62}$	$0.58^{+0.02}_{-0.02}$
	Flat XCDM	$0.25^{+0.16}_{-0.10}$	-	-	$-2.49^{+1.26}_{-1.59}$	-	$68.00^{+2.8}_{-2.8}$	$0.32^{+0.008}_{-0.008}$	$8.65^{+0.62}_{-0.57}$	$0.58^{+0.02}_{-0.02}$
	Non-flat XCDM	$0.29^{+0.26}_{-0.14}$	-	$0.11^{+0.66}_{-0.31}$	$-1.87^{+1.18}_{-2.05}$	-	$68.00^{+2.8}_{-2.8}$	$0.32^{+0.008}_{-0.008}$	$8.59^{+0.64}_{-0.65}$	$0.58^{+0.02}_{-0.02}$
	Flat ϕ CDM	$0.26^{+0.18}_{-0.11}$	-	-	-	$0.54^{+0.43}_{-0.38}$	$68.00^{+2.8}_{-2.8}$	$0.32^{+0.008}_{-0.008}$	$8.42^{+0.57}_{-0.57}$	$0.59^{+0.02}_{-0.02}$
	Non-flat ϕ CDM	$0.34^{+0.24}_{-0.16}$	-	$-0.30^{+0.44}_{-0.61}$	-	$0.55^{+0.43}_{-0.38}$	$68.00^{+2.8}_{-2.8}$	$0.32^{+0.008}_{-0.008}$	$8.45^{+0.57}_{-0.58}$	$0.59^{+0.02}_{-0.02}$

^a $\text{km s}^{-1} \text{Mpc}^{-1}$.

^b From Khadka & Ratra (2020).

Table 2. Marginalized one-dimensional best-fit parameters with 1σ confidence intervals for all models using 2019 and 2015 QSO data for the $H_0 = 73.24 \pm 1.74 \text{ km s}^{-1} \text{ Mpc}^{-1}$ prior.

Data	Model	Ω_{m0}	Ω_Λ	Ω_{k0}	ω_X	α	H_0^a	δ	β	γ
2019 QSO data	Flat Λ CDM	$0.64^{+0.21}_{-0.19}$	-	-	-	-	$73.23^{+1.73}_{-1.73}$	$0.23^{+0.004}_{-0.004}$	$7.56^{+0.33}_{-0.34}$	$0.62^{+0.01}_{-0.01}$
	Non-flat Λ CDM	$0.64^{+0.20}_{-0.17}$	$0.84^{+0.23}_{-0.34}$	$-0.48^{+0.51}_{-0.43}$	-	-	$73.25^{+1.72}_{-1.74}$	$0.23^{+0.004}_{-0.004}$	$7.89^{+0.41}_{-0.41}$	$0.61^{+0.01}_{-0.01}$
	Flat XCDM	$0.28^{+0.26}_{-0.14}$	-	-	$-9.48^{+4.59}_{-6.40}$	-	$73.26^{+1.74}_{-1.74}$	$0.23^{+0.004}_{-0.004}$	$7.76^{+0.31}_{-0.31}$	$0.62^{+0.01}_{-0.01}$
	Non-flat XCDM	$0.42^{+0.26}_{-0.19}$	-	$-0.12^{+0.14}_{-0.19}$	$-5.74^{+2.93}_{-6.36}$	-	$73.22^{+1.75}_{-1.72}$	$0.23^{+0.004}_{-0.004}$	$8.00^{+0.44}_{-0.45}$	$0.61^{+0.01}_{-0.01}$
	Flat ϕ CDM	$0.61^{+0.20}_{-0.20}$	-	-	-	$1.34^{+1.12}_{-0.96}$	$73.22^{+1.74}_{-1.73}$	$0.23^{+0.004}_{-0.004}$	$7.56^{+0.33}_{-0.34}$	$0.62^{+0.01}_{-0.01}$
	Non-flat ϕ CDM	$0.56^{+0.22}_{-0.20}$	-	$-0.34^{+0.37}_{-0.30}$	-	$1.28^{+1.12}_{-0.91}$	$73.21^{+1.73}_{-1.71}$	$0.23^{+0.004}_{-0.004}$	$7.74^{+0.40}_{-0.40}$	$0.61^{+0.01}_{-0.01}$
2015 QSO data ^b	Flat Λ CDM	$0.26^{+0.17}_{-0.11}$	-	-	-	-	$73.24^{+1.73}_{-1.73}$	$0.32^{+0.008}_{-0.008}$	$8.40^{+0.57}_{-0.57}$	$0.59^{+0.02}_{-0.02}$
	Non-flat Λ CDM	$0.24^{+0.16}_{-0.10}$	$0.93^{+0.18}_{-0.39}$	$-0.17^{+0.49}_{-0.34}$	-	-	$73.24^{+1.73}_{-1.73}$	$0.32^{+0.008}_{-0.008}$	$8.59^{+0.62}_{-0.62}$	$0.58^{+0.02}_{-0.02}$
	Flat XCDM	$0.25^{+0.16}_{-0.10}$	-	-	$-2.48^{+1.26}_{-1.59}$	-	$73.24^{+1.73}_{-1.74}$	$0.32^{+0.008}_{-0.008}$	$8.62^{+0.55}_{-0.56}$	$0.58^{+0.02}_{-0.02}$
	Non-flat XCDM	$0.29^{+0.25}_{-0.14}$	-	$0.10^{+0.62}_{-0.32}$	$-1.83^{+1.15}_{-2.02}$	-	$73.24^{+1.74}_{-1.74}$	$0.32^{+0.008}_{-0.008}$	$8.50^{+0.65}_{-0.64}$	$0.58^{+0.02}_{-0.02}$
	Flat ϕ CDM	$0.24^{+0.19}_{-0.12}$	-	-	-	$0.55^{+0.43}_{-0.38}$	$73.23^{+1.73}_{-1.73}$	$0.32^{+0.008}_{-0.008}$	$8.40^{+0.57}_{-0.57}$	$0.59^{+0.02}_{-0.02}$
	Non-flat ϕ CDM	$0.34^{+0.24}_{-0.17}$	-	$-0.30^{+0.62}_{-0.44}$	-	$0.55^{+0.43}_{-0.38}$	$73.26^{+1.74}_{-1.73}$	$0.32^{+0.008}_{-0.008}$	$8.42^{+0.57}_{-0.58}$	$0.59^{+0.02}_{-0.02}$

^a $\text{km s}^{-1} \text{Mpc}^{-1}$.

^b From Khadka & Ratra (2020).

to χ_{\min}^2 we also compute the Akaike Information Criterion

$$AIC = \chi_{\min}^2 + 2d, \quad (15)$$

as well as the Bayes Information Criterion

$$BIC = \chi_{\min}^2 + d \ln N, \quad (16)$$

where d is the number of free model parameters, N is the number of data points, and we define the degrees of freedom $\text{dof} = N - d$. The AIC and BIC penalize models with a larger number of free parameters.

5 RESULTS

5.1 Comparison of 2015 and 2019 QSO data constraints

QSO constraints obtained from the 2015 QSO data (Khadka & Ratra 2020) and the 2019 QSO data are largely consistent with each other but there are some differences, including some significant ones. Tables 1 and 2 list best-fit parameter

values and 1σ error bars determined from the 2019 and 2015 QSO data, for the two different H_0 priors. Best-fit values of parameters related to the $L_X - L_{UV}$ relation (δ , β , and γ) have changed in comparison to those obtained from the 2015 QSO data. β and γ are the intercept and slope of the $L_X - L_{UV}$ relation and their values do not tell how well this relation fits the data; the value of the intrinsic dispersion (δ) quantifies how well the $L_X - L_{UV}$ relation fits the data. The intrinsic dispersion of the $L_X - L_{UV}$ relation obtained from the 2015 QSO data and 2019 QSO data are 0.32 ± 0.008 and 0.23 ± 0.004 respectively, independent of H_0 prior and cosmological model. This shows that the 2019 QSO data are described by a tighter $L_X - L_{UV}$ relation than that for the 2015 data. This could be the result of the modified sample filtering process adopted in Risaliti & Lusso (2019).

In the case of cosmological parameters, the best-fit values of the equation of state parameter (ω_X) in the flat and non-flat XCDM parametrization obtained from the 2019 QSO data are significantly more negative than those obtained from the 2015 QSO data. From Tables 1 and 2, the

Table 3. Unmarginalized best-fit parameters of all models for the $H_0 = 68 \pm 2.8 \text{ km s}^{-1} \text{ Mpc}^{-1}$ prior.

Model	Data set	Ω_{m0}	Ω_Λ	Ω_{k0}	ω_X	α	H_0^a	δ	β	γ	χ^2_{\min}	dof	AIC
Flat Λ CDM	$H(z) + \text{BAO}^b$	0.29	0.71	-	-	-	67.56	-	-	-	32.47	40	36.47
	QSO	0.60	0.40	-	-	-	68.00	0.23	7.57	0.62	1606.99	1593	1616.99
	QSO + $H(z) + \text{BAO}$	0.30	0.70	-	-	-	68.03	0.23	7.12	0.64	1630.00	1635	1640.00
Non-flat Λ CDM	$H(z) + \text{BAO}^b$	0.30	0.70	0.00	-	-	68.23	-	-	-	27.05	39	33.05
	QSO	0.56	0.98	-0.54	-	-	68.00	0.23	7.93	0.61	1604.37	1592	1616.37
	QSO + $H(z) + \text{BAO}$	0.30	0.71	-0.01	-	-	68.77	0.23	7.11	0.64	1630.00	1634	1642.00
Flat XCDM	$H(z) + \text{BAO}^b$	0.30	0.70	-	-0.96	-	67.24	-	-	-	27.29	39	33.29
	QSO	0.20	0.80	-	-7.08	-	68.00	0.23	7.66	0.62	1603.01	1592	1615.01
	QSO + $H(z) + \text{BAO}$	0.30	0.70	-	-0.96	-	67.30	0.23	7.13	0.64	1629.76	1634	1641.76
Non-flat XCDM	$H(z) + \text{BAO}^b$	0.32	-	-0.23	-0.74	-	67.42	-	-	-	24.91	38	32.91
	QSO	0.29	-	-0.15	-4.87	-	68.00	0.23	8.10	0.61	1604.29	1591	1618.29
	QSO + $H(z) + \text{BAO}$	0.33	-	-0.40	-0.66	-	67.43	0.23	7.54	0.62	1628.82	1633	1642.82
Flat ϕ CDM	$H(z) + \text{BAO}^b$	0.32	-	-	-	0.10	67.23	-	-	-	27.42	39	33.42
	QSO	0.82	-	-	-	2.03	68.19	0.23	7.77	0.61	1589.32	1592	1601.32
	QSO + $H(z) + \text{BAO}$	0.30	-	-	-	0.09	67.62	0.23	7.21	0.64	1633.40	1634	1645.40
Non-flat ϕ CDM	$H(z) + \text{BAO}^b$	0.33	-	-0.20	-	1.20	65.86	-	-	-	25.04	38	33.04
	QSO	0.56	-	-0.55	-	0.08	67.63	0.23	7.99	0.61	1626.71	1591	1640.71
	QSO + $H(z) + \text{BAO}$	0.32	-	-0.41	-	1.51	67.81	0.23	7.54	0.62	1624.67	1633	1639.67

^a $\text{km s}^{-1} \text{Mpc}^{-1}$.^b From Khadka & Ratra (2020).**Table 4.** Unmarginalized best-fit parameters of all models for the $H_0 = 73.24 \pm 1.74 \text{ km s}^{-1} \text{ Mpc}^{-1}$ prior.

Model	Data set	Ω_{m0}	Ω_Λ	Ω_{k0}	ω_X	α	H_0^a	δ	β	γ	χ^2_{\min}	dof	AIC
Flat Λ CDM	$H(z) + \text{BAO}^b$	0.30	0.70	-	-	-	69.11	-	-	-	33.76	40	38.76
	QSO	0.60	0.40	-	-	-	73.24	0.23	7.54	0.62	1606.03	1593	1616.03
	QSO + $H(z) + \text{BAO}$	0.31	0.69	-	-	-	69.15	0.23	7.12	0.64	1636.26	1635	1646.26
Non-flat Λ CDM	$H(z) + \text{BAO}^b$	0.30	0.78	-0.08	-	-	71.56	-	-	-	28.80	39	34.80
	QSO	0.56	0.98	-0.54	-	-	73.24	0.23	7.91	0.61	1604.37	1592	1616.37
	QSO + $H(z) + \text{BAO}$	0.31	0.79	-0.1	-	-	71.85	0.23	7.16	0.64	1631.48	1634	1643.48
Flat XCDM	$H(z) + \text{BAO}^b$	0.29	0.71	-	-1.14	-	71.27	-	-	-	30.68	39	36.68
	QSO	0.20	0.80	-	-7.08	-	73.24	0.23	7.64	0.62	1603.01	1592	1615.01
	QSO + $H(z) + \text{BAO}$	0.30	0.70	-	-1.14	-	71.32	0.23	7.13	0.64	1633.16	1634	1645.16
Non-flat XCDM	$H(z) + \text{BAO}^b$	0.32	-	-0.21	-0.85	-	71.22	-	-	-	28.17	38	36.17
	QSO	0.29	-	-0.15	-4.87	-	73.24	0.23	8.08	0.61	1604.29	1591	1618.29
	QSO + $H(z) + \text{BAO}$	0.33	-	-0.38	-0.74	-	71.11	0.23	7.47	0.63	1632.09	1633	1646.09
Flat ϕ CDM	$H(z) + \text{BAO}^b$	0.33	-	-	-	0.09	69.31	-	-	-	33.36	39	39.36
	QSO	0.61	-	-	-	0.26	73.11	0.23	7.53	0.62	1601.22	1592	1613.22
	QSO + $H(z) + \text{BAO}$	0.31	-	-	-	0.003	69.40	0.23	7.17	0.63	1636.87	1634	1638.87
Non-flat ϕ CDM	$H(z) + \text{BAO}^b$	0.32	-	-0.22	-	1.14	69.23	-	-	-	27.62	38	35.62
	QSO	0.49	-	-0.53	-	0.01	72.98	0.23	7.78	0.61	1606.10	1591	1620.10
	QSO + $H(z) + \text{BAO}$	0.32	-	-0.39	-	1.09	71.22	0.23	7.47	0.63	1640.19	1633	1654.19

^a $\text{km s}^{-1} \text{Mpc}^{-1}$.^b From Khadka & Ratra (2020).

2019 QSO data indicate that the dark energy density in the XCDM parametrization increases with time. Another notable difference between the 2015 QSO data and the 2019 QSO data is that the 2015 QSO data favor a smaller value of the matter density parameter ($\Omega_{m0} \sim 0.3$), consistent with values obtained from other cosmological probes, while the 2019 QSO data favor a larger value of the matter density pa-

rameter ($\Omega_{m0} > 0.42$), with the exception of the flat XCDM case where the 2019 data also favor $\Omega_{m0} \sim 0.30$. This can be seen in Tables 1 and 2 and Fig. 2 which shows the constraints for the flat Λ CDM model with the $H_0 = 68 \pm 2.8 \text{ km s}^{-1} \text{Mpc}^{-1}$ prior. We note that both high redshift cosmic microwave background anisotropy data (Planck Collaboration 2018) and low redshift, $z < 2.5$, data (Chen &

Table 5. Marginalized one-dimensional best-fit parameters with 1σ confidence intervals for all models using BAO and $H(z)$ data (from Khadka & Ratra 2020).

H_0^a prior	Model	Ω_{m0}	Ω_Λ	Ω_{k0}	ω_X	α	H_0^a
$H_0 = 68 \pm 2.8$	Flat Λ CDM	$0.29^{+0.01}_{-0.01}$	-	-	-	-	$67.58^{+0.85}_{-0.85}$
	Non-flat Λ CDM	$0.30^{+0.01}_{-0.01}$	$0.70^{+0.05}_{-0.06}$	$0.00^{+0.06}_{-0.07}$	-	-	$68.17^{+1.80}_{-1.79}$
	Flat XCDM	$0.30^{+0.02}_{-0.02}$	-	-	$-0.97^{+0.09}_{-0.09}$	-	$67.39^{+1.87}_{-1.84}$
	Non-flat XCDM	$0.32^{+0.02}_{-0.02}$	-	$-0.18^{+0.17}_{-0.21}$	$-0.77^{+0.11}_{-0.17}$	-	$67.42^{+1.84}_{-1.80}$
	Flat ϕ CDM	$0.31^{+0.01}_{-0.01}$	-	-	-	$0.20^{+0.21}_{-0.13}$	$66.57^{+1.31}_{-1.45}$
	Non-flat ϕ CDM	$0.31^{+0.01}_{-0.01}$	-	$-0.20^{+0.13}_{-0.17}$	-	$0.86^{+0.53}_{-0.49}$	$67.69^{+1.45}_{-1.74}$
$H_0 = 73.24 \pm 1.74$	Flat Λ CDM	$0.31^{+0.01}_{-0.01}$	-	-	-	-	$69.12^{+0.81}_{-0.80}$
	Non-flat Λ CDM	$0.30^{+0.01}_{-0.01}$	$0.78^{+0.04}_{-0.04}$	$-0.08^{+0.05}_{-0.05}$	-	-	$71.51^{+1.41}_{-1.40}$
	Flat XCDM	$0.29^{+0.01}_{-0.01}$	-	-	$-1.14^{+0.08}_{-0.08}$	-	$71.32^{+1.48}_{-1.46}$
	Non-flat XCDM	$0.32^{+0.02}_{-0.02}$	-	$-0.17^{+0.16}_{-0.19}$	$-0.88^{+0.14}_{-0.21}$	-	$71.23^{+1.46}_{-1.46}$
	Flat ϕ CDM	$0.31^{+0.01}_{-0.01}$	-	-	-	$0.07^{+0.09}_{-0.04}$	$68.91^{+0.98}_{-1.00}$
	Non-flat ϕ CDM	$0.32^{+0.01}_{-0.01}$	-	$-0.25^{+0.12}_{-0.16}$	-	$0.68^{+0.53}_{-0.46}$	$71.14^{+1.39}_{-1.38}$

^a km s⁻¹Mpc⁻¹.

Table 6. Marginalized one-dimensional best-fit parameters with 1σ confidence intervals for all models using QSO+ $H(z)$ +BAO data.

H_0^a prior	Model	Ω_{m0}	Ω_Λ	Ω_{k0}	ω_X	α	H_0^a	δ	β	γ
$H_0 = 68 \pm 2.8$	Flat Λ CDM	$0.30^{+0.01}_{-0.01}$	$0.70^{+0.01}_{-0.05}$	-	-	-	$68.04^{+0.84}_{-0.84}$	$0.23^{+0.004}_{-0.004}$	$7.11^{+0.27}_{-0.27}$	$0.64^{+0.00}_{-0.00}$
	Non-flat Λ CDM	$0.30^{+0.01}_{-0.01}$	$0.71^{+0.05}_{-0.06}$	$-0.01^{+0.06}_{-0.07}$	-	-	$68.70^{+1.78}_{-1.79}$	$0.23^{+0.004}_{-0.004}$	$7.11^{+0.27}_{-0.27}$	$0.64^{+0.00}_{-0.00}$
	Flat XCDM	$0.30^{+0.02}_{-0.02}$	-	-	$-0.96^{+0.09}_{-0.09}$	-	$67.41^{+1.88}_{-1.83}$	$0.23^{+0.004}_{-0.004}$	$7.12^{+0.27}_{-0.27}$	$0.64^{+0.00}_{-0.00}$
	Non-flat XCDM	$0.33^{+0.02}_{-0.02}$	-	$-0.34^{+0.18}_{-0.18}$	$-0.69^{+0.07}_{-0.11}$	-	$67.48^{+1.81}_{-1.77}$	$0.23^{+0.004}_{-0.004}$	$7.47^{+0.33}_{-0.33}$	$0.63^{+0.01}_{-0.01}$
	Flat ϕ CDM	$0.31^{+0.01}_{-0.01}$	-	-	-	$0.20^{+0.21}_{-0.14}$	$66.76^{+1.36}_{-1.49}$	$0.23^{+0.004}_{-0.004}$	$7.16^{+0.27}_{-0.27}$	$0.64^{+0.00}_{-0.00}$
	Non-flat ϕ CDM	$0.32^{+0.01}_{-0.01}$	-	$-0.32^{+0.16}_{-0.16}$	-	$1.21^{+0.47}_{-0.53}$	$67.90^{+1.72}_{-1.73}$	$0.23^{+0.004}_{-0.004}$	$7.47^{+0.33}_{-0.32}$	$0.63^{+0.01}_{-0.01}$
$H_0 = 73.24 \pm 1.74$	Flat Λ CDM	$0.31^{+0.01}_{-0.01}$	$0.69^{+0.01}_{-0.01}$	-	-	-	$69.16^{+0.81}_{-0.81}$	$0.23^{+0.004}_{-0.004}$	$7.12^{+0.27}_{-0.27}$	$0.64^{+0.00}_{-0.00}$
	Non-flat Λ CDM	$0.31^{+0.01}_{-0.01}$	$0.78^{+0.04}_{-0.04}$	$-0.09^{+0.05}_{-0.05}$	-	-	$71.79^{+1.40}_{-1.39}$	$0.23^{+0.004}_{-0.004}$	$7.16^{+0.27}_{-0.27}$	$0.64^{+0.00}_{-0.00}$
	Flat XCDM	$0.30^{+0.02}_{-0.02}$	-	-	$-1.14^{+0.08}_{-0.08}$	-	$71.38^{+1.51}_{-1.50}$	$0.23^{+0.004}_{-0.004}$	$7.09^{+0.27}_{-0.27}$	$0.64^{+0.00}_{-0.00}$
	Non-flat XCDM	$0.33^{+0.02}_{-0.02}$	-	$-0.31^{+0.17}_{-0.18}$	$-0.77^{+0.09}_{-0.15}$	-	$71.17^{+1.43}_{-1.43}$	$0.23^{+0.004}_{-0.004}$	$7.41^{+0.34}_{-0.33}$	$0.63^{+0.01}_{-0.01}$
	Flat ϕ CDM	$0.31^{+0.01}_{-0.01}$	-	-	-	$0.06^{+0.09}_{-0.05}$	$69.09^{+1.01}_{-1.02}$	$0.23^{+0.004}_{-0.004}$	$7.15^{+0.27}_{-0.27}$	$0.64^{+0.00}_{-0.00}$
	Non-flat ϕ CDM	$0.32^{+0.01}_{-0.01}$	-	$-0.35^{+0.15}_{-0.15}$	-	$0.98^{+0.44}_{-0.50}$	$71.24^{+1.40}_{-1.39}$	$0.23^{+0.004}_{-0.004}$	$7.47^{+0.33}_{-0.32}$	$0.63^{+0.01}_{-0.01}$

^a km s⁻¹Mpc⁻¹.

Ratra 2003; Park & Ratra 2018c) are both consistent with $\Omega_{m0} \sim 0.30$ in a variety of different cosmological models, so it is somewhat surprising that the 2019 QSO data at $z \sim 2-5$ largely favor $\Omega_{m0} \sim 0.4-0.6$.⁹ It is probably more likely that this larger Ω_{m0} is a reflection of something related to the

⁹ We note that our result differs significantly from Melia (2019), Table 1, who finds $\Omega_{m0} = 0.31 \pm 0.05$ in the flat Λ CDM model from the 2019 QSO data (which is identical to the Risaliti & Lusso (2019) value of $\Omega_{m0} = 0.30 \pm 0.05$ determined from the $z < 1.4$ 2019 QSO data with the JLA supernovae data). The more approximate analyses of Yang et al. (2019) and Velten & Gomes (2020) find larger Ω_{m0} values, as does the analyses of Wei & Melia (2020) in which they use $H(z)$ data to calibrate the 2019 QSO data. From their more approximate analyses Velten & Gomes (2020) conclude that the 2019 QSO data are incompatible with a currently accelerating cosmological expansion. Our more accurate analyses shows that while part of the probability lies in the non-accelerating region of cosmological parameter space, in most models we study here a significant part of the probability lies in the accelerating part of cosmological parameter space, see Fig. 2 for the flat Λ CDM case and later figures for other models, and so it is incorrect to claim that the 2019 QSO data are incompatible with currently accelerated cosmological expansion.

2019 QSO data than an indication of the invalidity of the Λ CDM scenario. A larger value of the matter density parameter gives a lower distance modulus for an astrophysical object at any redshift. So the Hubble diagram of quasars obtained from the 2019 QSO data lies below the Hubble diagram obtained from the concordance model (flat Λ CDM) with matter density parameter $\Omega_{m0} = 0.30$ and the difference increases with increasing redshift. This can be seen in Fig. 3.

5.2 2019 QSO constraints

The observed correlation between a quasar's X-ray and UV measurements, eq. (10), provides an opportunity to use QSO data to constrain cosmological parameters. The global intrinsic dispersion (δ) obtained here is smaller than that of Khadka & Ratra (2020) for the 2015 QSO data but it still is large and so cosmological parameter determination done using these data is not as precise as that done using other data such as BAO or $H(z)$ measurements. But the main advantage of using the quasar sample is that it covers a very large redshift range, part of which is not well probed by other data, so it provides the opportunity of testing cosmological models

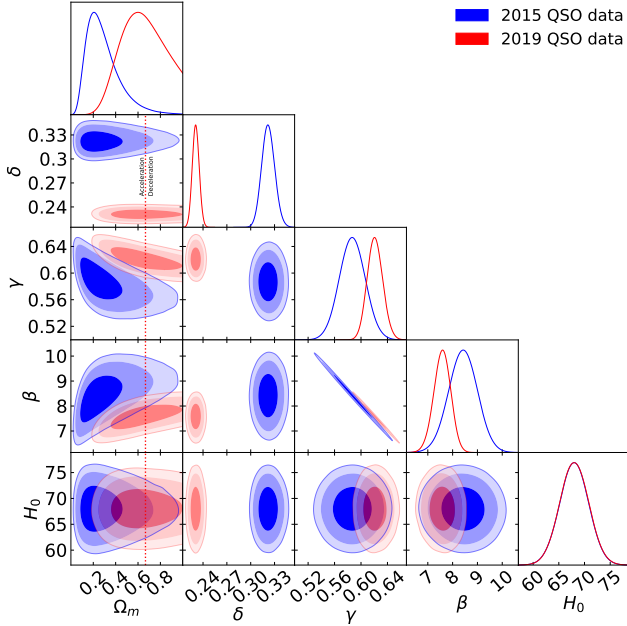


Figure 2. Flat Λ CDM model constraints from the 2015 QSO data (blue) and the 2019 QSO data (red) for the $H_0 = 68 \pm 2.8$ $\text{km s}^{-1}\text{Mpc}^{-1}$ prior. Shown are 1, 2, and 3σ confidence contours and one-dimensional likelihoods for all free parameters. The red dotted vertical straight lines in the left column of panels are zero acceleration lines, with the current cosmological expansion accelerating to the left of the line where $\Omega_{m0} < 0.67$.

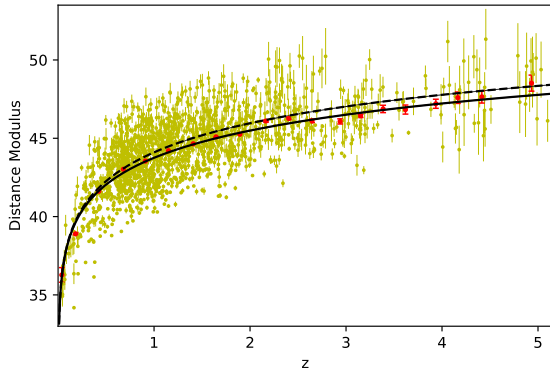


Figure 3. Hubble diagram of quasars using the flat Λ CDM model. Black solid line is the best-fit flat Λ CDM model line from the 2019 QSO data. Red points are the means and uncertainties on the mean of the distance modulus in narrow redshift bins for the quasar data. These averages do not play a role in the statistical analysis and are shown only for visualization purposes. The black dashed line shows a flat Λ CDM model with $\Omega_{m0} = 0.30$.

in a new, higher, redshift range, and it is likely that future, improved, QSO data will provide significant and interesting constraints on cosmological parameters.

The QSO data determined cosmological parameter results are given in Tables 1–4. The unmarginalized best-fit parameters are listed in the Tables 3 and 4 for the $H_0 = 68 \pm 2.8$ $\text{km s}^{-1}\text{Mpc}^{-1}$ and 73.24 ± 1.74 $\text{km s}^{-1}\text{Mpc}^{-1}$ priors respectively. The two-dimensional confidence contours and the

one-dimensional likelihoods are shown in grey in the left panels of Figs. 4–15. The cosmological parameter constraints are almost insensitive to the H_0 prior used. For the QSO data, from Tables 1 and 2, the non-relativistic matter density parameter is measured to lie in the range $\Omega_{m0} = 0.28^{+0.26}_{-0.19}$ to $0.64^{+0.21}_{-0.17}$ ($0.42^{+0.26}_{-0.18}$ to $0.64^{+0.20}_{-0.17}$) for flat (non-flat) models and the $H_0 = 68 \pm 2.8$ $\text{km s}^{-1}\text{Mpc}^{-1}$ prior and to lie in the range $\Omega_{m0} = 0.28^{+0.26}_{-0.14}$ to $0.64^{+0.21}_{-0.19}$ ($0.42^{+0.26}_{-0.19}$ to $0.64^{+0.20}_{-0.17}$) for flat (non-flat) models and the $H_0 = 73.24 \pm 1.74$ $\text{km s}^{-1}\text{Mpc}^{-1}$ prior. While the errors are large, the values of Ω_{m0} obtained from the 2019 QSO data in most models are larger than those obtained from other cosmological probes.

From Tables 1 and 2, for the non-flat Λ CDM model the curvature energy density parameter is measured to be $\Omega_{k0} = -0.48^{+0.51}_{-0.43}$ ($-0.48^{+0.51}_{-0.43}$) for the $H_0 = 68 \pm 2.8$ $\text{km s}^{-1}\text{Mpc}^{-1}$ (73.24 ± 1.74 $\text{km s}^{-1}\text{Mpc}^{-1}$) prior. For the non-flat XCDM model we find $\Omega_{k0} = -0.12^{+0.15}_{-0.19}$ ($-0.12^{+0.15}_{-0.19}$) for the $H_0 = 68 \pm 2.8$ $\text{km s}^{-1}\text{Mpc}^{-1}$ (73.24 ± 1.74 $\text{km s}^{-1}\text{Mpc}^{-1}$) prior. For the non-flat ϕ CDM model we find $\Omega_{k0} = -0.29^{+0.35}_{-0.27}$ ($-0.34^{+0.37}_{-0.30}$) for the $H_0 = 68 \pm 2.8$ $\text{km s}^{-1}\text{Mpc}^{-1}$ (73.24 ± 1.74 $\text{km s}^{-1}\text{Mpc}^{-1}$) prior. In all models closed spatial hypersurfaces are weakly favored.

From Tables 1 and 2, for the flat (non-flat) Λ CDM model the dark energy density parameter is $\Omega_{\Lambda} = 0.36^{+0.19}_{-0.21}$ ($0.84^{+0.23}_{-0.34}$) for both $H_0 = 68 \pm 2.8$ $\text{km s}^{-1}\text{Mpc}^{-1}$ and 73.24 ± 1.74 $\text{km s}^{-1}\text{Mpc}^{-1}$ priors.

The equation of state parameter for the flat (non-flat) XCDM model is $\omega_X = -9.57^{+4.60}_{-6.31}$ ($-5.74^{+2.97}_{-6.43}$) for the $H_0 = 68 \pm 2.8$ $\text{km s}^{-1}\text{Mpc}^{-1}$ prior and $-9.48^{+4.59}_{-6.40}$ ($-5.74^{+2.93}_{-6.36}$) for the 73.24 ± 1.74 $\text{km s}^{-1}\text{Mpc}^{-1}$ prior. For both priors ω_X is very low in comparison to the 2015 QSO data values obtained in Khadka & Ratra (2020). In the XCDM parametrization the 2019 QSO data favors dark energy density that increases with time. The α parameter in the flat (non-flat) ϕ CDM model is $\alpha = 1.30^{+1.11}_{-0.94}$ ($1.29^{+1.13}_{-0.93}$) for the $H_0 = 68 \pm 2.8$ $\text{km s}^{-1}\text{Mpc}^{-1}$ prior and $1.34^{+1.12}_{-0.96}$ ($1.28^{+1.12}_{-0.91}$) for the 73.24 ± 1.74 $\text{km s}^{-1}\text{Mpc}^{-1}$ prior. In both models dynamical dark energy is favored.

From the χ^2_{\min} , AIC, and BIC values for the QSO data listed in Tables 3 and 4, independent of H_0 prior, the flat ϕ CDM model is most favored while the non-flat ϕ CDM model is least favored. However, given the issue raised above about the 2019 QSO data, it is inappropriate to give much weight to these findings.

The cosmological parameters obtained by using the 2019 QSO data have relatively high uncertainty for all models so they are mostly consistent with the results obtained by using the BAO + $H(z)$ data set, as can be seen from Figs. 4–15.

5.3 QSO + $H(z)$ + BAO constraints

Results for the $H(z)$ + BAO data set are listed in Tables 3–5 and one-dimensional distributions and two-dimensional contours are shown in red in Figs. 4–15. Figures 4–15 show that constraints from the QSO data alone and those from the $H(z)$ + BAO data are mostly consistent with each other. So it is not unreasonable to do joint analyses of the QSO + $H(z)$ + BAO data. Results from this joint analysis are given in

Tables 1, 2, and 6. The QSO + $H(z)$ + BAO one-dimensional likelihoods and two-dimensional confidence contours for all free parameters are shown in blue in Figs. 4–15. The updated QSO data don't significantly tighten the $H(z)$ + BAO data contours except in the cases of the non-flat XCDM parametrization and the non-flat ϕ CDM model (Figs. 10, 11, 14, and 15). Another noticeable result is that adding the QSO data to the $H(z)$ + BAO data results in the shifting of one-dimensional likelihood distribution of the matter density parameter towards higher values in most cosmological models studied here.

From joint analyses of the QSO + $H(z)$ + BAO data, from Table 6, the non-relativistic matter density parameter lies in the range $\Omega_{m0} = 0.30 \pm 0.02$ to 0.31 ± 0.01 ($\Omega_{m0} = 0.30 \pm 0.01$ to 0.33 ± 0.02) for flat (non-flat) models and the $H_0 = 68 \pm 2.8$ km s⁻¹Mpc⁻¹ prior and lies in the range $\Omega_{m0} = 0.30^{+0.02}_{-0.01}$ to 0.31 ± 0.01 ($\Omega_{m0} = 0.31 \pm 0.01$ to 0.33 ± 0.02) for flat (non-flat) models and the $H_0 = 73.24 \pm 1.74$ km s⁻¹Mpc⁻¹ prior. In some cases these results differ slightly from the $H(z)$ + BAO data results of Table 5, being shifted to slightly larger values. These results are consistent with those derived using other cosmological data.

The Hubble constant lies in the range $H_0 = 66.76^{+1.36}_{-1.49}$ to $68.04^{+0.84}_{-0.84}$ ($H_0 = 67.48^{+1.81}_{-1.77}$ to $68.70^{+1.78}_{-1.79}$) km s⁻¹Mpc⁻¹ for flat (non-flat) models and the $H_0 = 68 \pm 2.8$ km s⁻¹Mpc⁻¹ prior and lies in the range $H_0 = 69.09^{+1.01}_{-1.02}$ to $71.38^{+1.51}_{-1.50}$ ($H_0 = 71.17^{+1.45}_{-1.43}$ to $71.79^{+1.40}_{-1.39}$) km s⁻¹Mpc⁻¹ for flat (non-flat) models and the $H_0 = 73.24 \pm 1.74$ km s⁻¹Mpc⁻¹ prior. Not unexpectedly, for the $H_0 = 73.24 \pm 1.74$ km s⁻¹Mpc⁻¹ prior the measured value of H_0 is pulled below the prior value because the BAO and $H(z)$ data favor a lower H_0 . In most cases the H_0 error bars have increased in comparison to those derived using the 2015 QSO + $H(z)$ + BAO data in Khadka & Ratra (2020).

In all models, except for non-flat Λ CDM with the $H_0 = 68 \pm 2.8$ km s⁻¹Mpc⁻¹ prior, closed spatial hypersurfaces are favored at about 2σ . For the non-flat Λ CDM model the curvature energy density parameter is $\Omega_{k0} = -0.01^{+0.06}_{-0.07}$ and -0.09 ± 0.05 for the $H_0 = 68 \pm 2.8$ km s⁻¹Mpc⁻¹ and 73.24 ± 1.74 km s⁻¹Mpc⁻¹ priors respectively. Values of curvature energy density parameter obtained for non-flat dynamical dark energy cosmological models are significantly higher than those obtained in the non-flat Λ CDM model. The curvature energy density parameter is $\Omega_{k0} = -0.34 \pm 0.18$ and -0.32 ± 0.16 for the non-flat XCDM and non-flat ϕ CDM models for the $H_0 = 68 \pm 2.8$ km s⁻¹Mpc⁻¹ prior and $\Omega_{k0} = -0.31^{+0.17}_{-0.18}$ and -0.35 ± 0.15 for the non-flat XCDM and non-flat ϕ CDM models for the $H_0 = 73.24 \pm 1.74$ km s⁻¹Mpc⁻¹ prior. This preference for closed spatial hypersurfaces is largely driven by the $H(z)$ + BAO data (Park & Ratra 2018c; Ryan et al. 2019).

From Table 6, for the flat (non-flat) Λ CDM model the dark energy density parameter is $\Omega_{\Lambda} = 0.70 \pm 0.01$ ($0.71^{+0.05}_{-0.06}$) for the $H_0 = 68 \pm 2.8$ km s⁻¹Mpc⁻¹ prior and $\Omega_{\Lambda} = 0.69 \pm 0.01$ (0.78 ± 0.04) for the $H_0 = 73.24 \pm 1.74$ km s⁻¹Mpc⁻¹ prior.

The equation of state parameter for the flat (non-flat) XCDM parametrization is $\omega_X = -0.96 \pm 0.09$ ($-0.69^{+0.07}_{-0.11}$) for the $H_0 = 68 \pm 2.8$ km s⁻¹Mpc⁻¹ prior and -1.14 ± 0.08 ($-0.77^{+0.09}_{-0.15}$) for the 73.24 ± 1.74 km s⁻¹Mpc⁻¹ prior. So this set of data suggests decreasing XCDM dark energy density with time, except for the flat XCDM parametrization

with 73.24 ± 1.74 km s⁻¹Mpc⁻¹ prior, where it favors at almost 2σ , a XCDM dark energy density that increases with time. The value of the α parameter in the flat (non-flat) ϕ CDM model is $\alpha = 0.20^{+0.21}_{-0.14}$ ($1.21^{+0.47}_{-0.53}$) for the $H_0 = 68 \pm 2.8$ km s⁻¹Mpc⁻¹ prior and $0.06^{+0.09}_{-0.05}$ ($0.98^{+0.44}_{-0.50}$) for the 73.24 ± 1.74 km s⁻¹Mpc⁻¹ prior. All eight XCDM and ϕ CDM cases favor dynamical dark energy over a Λ at between 0.4σ and 4.4σ . Other data also favor mild dark energy dynamics (Ooba et al. 2019; Park & Ratra 2018b, 2019).

Unlike the case for the 2019 QSO only data, for the QSO + $H(z)$ + BAO data the χ^2_{\min} , AIC, and BIC values are relatively similar for all models.

6 CONCLUSION

Following Risaliti & Lusso (2019) we have used the correlation between X-ray and UV monochromatic luminosities in selected $z \sim 0 - 5$ quasars to constrain cosmological parameters in six different models. These selected quasars can be used as standard candles for cosmological model testing at redshifts $z \sim 2.5 - 5$ that are not yet widely accessible through other cosmological probes. Our analyses of these data in six different cosmological models shows that parameters of the $L_X - L_{UV}$ relation, i.e., the intercept β , the slope γ , and the intrinsic dispersion δ , are only weakly dependent on the cosmological model assumed in the analysis. This reinforces the finding of Risaliti & Lusso (2015) that carefully-selected quasar flux measurements can be used as standard candles.

The 2019 QSO data constraints are mostly consistent with joint analysis of BAO distance and Hubble parameter measurements, as also found in Khadka & Ratra (2020) for the 2015 QSO data. We find that joint analysis of 2019 QSO and $H(z)$ + BAO data slightly tightens the $H(z)$ + BAO data constraints in the non-flat XCDM parametrization and the non-flat ϕ CDM model but not in the other four models. Overall, adding the 2019 QSO data to the $H(z)$ + BAO data has a less significant tightening effect than what was found for the 2015 QSO data (Khadka & Ratra 2020).

The value of the matter density parameter obtained by using the 2019 QSO data is typically greater than 0.5, Tables 1 and 2, which is significantly larger than values obtained using other cosmological probes, such as BAO, $H(z)$, Type Ia supernovae, and CMB anisotropy observations. Due to the larger Ω_{m0} from the QSO data, in joint analyses of the QSO + $H(z)$ + BAO data the matter density parameter shifts to slightly larger values than the $H(z)$ + BAO data Ω_{m0} values in a number of the models. The larger 2019 QSO data Ω_{m0} values are likely the cause of the tension between the 2019 QSO data and the $\Omega_{m0} = 0.3$ flat Λ CDM model that is discussed in Risaliti & Lusso (2019) and Lusso et al. (2019). It is probably more likely that this tension has to do with the $z \sim 2 - 5$ 2019 QSO data than with the invalidity of the $\Omega_{m0} = 0.3$ flat Λ CDM model. This is because almost all cosmological data, at $z \sim 0 - 2.5$ and at $z \sim 1100$, are consistent with $\Omega_{m0} \cong 0.3$. It is of great interest to understand why the 2019 QSO data favours a larger value of Ω_{m0} .

The joint QSO + $H(z)$ + BAO data constraints are consistent with the current standard model, although they weakly favour closed over flat spatial hypersurfaces and dynamical dark energy over a cosmological constant. Since

they probe a little-studied, higher redshift region of the universe, future, improved QSO data will likely provide very useful, more restrictive, constraints on cosmological parameters, and should help to measure the dynamics of dark energy and the geometry of space.

ACKNOWLEDGEMENTS

We thank Elisabeta Lusso for her generous help, and Lado Samushia, Javier De Cruz, Shulei Cao, and Joe Ryan for useful discussions. We are grateful to the Beocat Research Cluster at Kansas State University team. This research was supported in part by DOE grant DE-SC0019038.

REFERENCES

- Alam S., et al., 2017, *MNRAS*, 470, 2617
 Avni Y., Tananbaum H., 1986, *ApJ*, 305, 83
 Avsajanishvili O., Samushia L., Arhipova N. A., Kahniashvili T., 2015, preprint, (arXiv:1511.09317)
 Bisogni S., Risaliti G., Lusso E., 2017, preprint, (arXiv:1712.07515)
 Campanelli L. et al., 2012, *Eur. Phys. J. C*, C72, 2218
 Chen G., Gott III J. R., Ratra B., 2003, *PASP*, 115, 1269
 Chen G., Ratra B., 2003, *PASP*, 115, 1143
 Chen G., Ratra B., 2004, *ApJ*, 612, L1
 Chen G., Ratra B., 2011a, *PASP*, 123, 1127
 Chen Y., Ratra B., 2011b, *Physics Letters B*, 703, 406
 Chen Y., Kumar S., Ratra B., 2017, *ApJ*, 835, 86
 Chen Y. et al., 2016, *ApJ*, 829, 61
 Coley A. A., 2019, preprint, (arXiv:1905.04588)
 Cuceu A., Farr J., Lemos P., Font-Ribera A., 2019, *JCAP*, 1910, 044
 Demianski M., Piedipalumbo E., Sawant D., Amati L., 2019, preprint, (arXiv: 1911.08228)
 DES Collaboration, 2018a, *Phys. Rev. D*, 98, 043526
 DES Collaboration, 2018b, *MNRAS*, 480, 3879
 Dhawan S., Jha S. W., Leibundgut B. 2017, *A&A*, 609, A72
 Di Valentino E., Melchiorri A., Silk J., 2020, preprint, (arXiv:2003.04935)
 Domínguez A. et al., 2019, *ApJ*, 885, 137
 Efstathiou G., Gratton S., 2020, preprint, (arXiv:2002.06892)
 Eingorn M., Yukselci E. A., Zhuk A., 2019, *EPJC*, C79, 655
 Farooq O., Crandall S., Ratra B., 2013, *Physics Letters B*, 726, 72
 Farooq O., Madiyar F., Crandall S, Ratra B., 2017, *ApJ*, 835, 26
 Farooq O., Mania D., Ratra B., 2015, *ApSS*, 357, 11
 Farooq O., Ratra B., 2013, *ApJ*, 766, L7
 Fernández Arenas D., et al., 2018, *MNRAS*, 474, 1250
 Foreman-Mackey D., Hogg D. W., Lang D., Goodman J., 2013, *PASP*, 125, 306
 Freedman W. L. et al., 2019, *ApJ*, 882, 34
 Freedman W. L. et al., 2020, *ApJ*, 891, 57
 Geng C. Q., Hsu Y. T., Yin L., Zhang K., 2020, preprint, (arXiv: 2002.05290)
 Giambó R., Miritzis J., Pezzola A., 2019, preprint, (arXiv: 1905.01742)
 Grupe D., Komossa S., Leighly K. M., Page K. L., 2010, *ApJS*, 187, 64
 Gómez-Valent A. & Amendola L., 2018, *JCAP*, 1804, 051
 González-Morán et al., 2019, *MNRAS*, 487, 4669
 Gott III J. R., Vogeley M. S., Podariu S., Ratra B., 2001, *ApJ*, 549, 1
 Handley W., 2019, *Phys.Rev. D*, 100, 123517
 Haridasu B. S., Luković V. V., Moresco M., Vittorio N., 2018, *JCAP*, 1810, 015
 Jesus F. J., Valentim R., Moraes P. H. R. S., Malheiro M., 2019, preprint, (arXiv:1907.01033)
 Just D. W. et al., 2007, *ApJ*, 665, 1004
 Khadka N., Ratra B., 2020, *MNRAS*, 492, 4456
 Kumar D. et al., 2020, preprint, (arXiv: 2002.06354)
 Lamb D. Q., Reichart D. E., 2000, *ApJ*, 536, 1
 Lazkoz R., Francisco S. N. Lobo, Ortiz-Baõ M., Salzano V., 2019, *Phys.Rev. D*, 100, 104027
 Li E. K., Du M., Xu L., 2019, *MNRAS*, 491, 4960
 Lin W., Ishak M., 2019, preprint, (arXiv: 1909.10991)
 Lindner M., Max K., Platscher M., Rezacek J., 2020, preprint, (arXiv: 2002.01487)
 López-Corredoira M., Melia F., Lusso E., Risaliti G., 2016, *International Journal of Modern Physics D*, 25, 05
 Lusso E. et al., 2010, *A & A*, 512, A34
 Lusso E. et al., 2019, *A&A*, 628, L4
 Mania D., Ratra B., 2012, *Phys.Lett.B*, 715, 9
 Martinelli M., Tutusaus I., 2019, *Symmetry*, 08, 986
 Mehrabi A., Basilakos S., 2020, preprint, (arXiv: 2002.12577)
 Melia F., 2019, *MNRAS*, 489, 517
 Mitra S., Park C.-G, Choudhury T. R., Ratra B., 2019, *MNRAS*, 487, 5118
 Ooba J., Ratra B., Sugiyama N., 2018a, *ApJ*, 864, 80
 Ooba J., Ratra B., Sugiyama N., 2018b, *ApJ*, 866, 68
 Ooba J., Ratra B., Sugiyama N., 2018c, *ApJ*, 869, 34
 Ooba J., Ratra B., Sugiyama N., 2019, *ApSS*, 364, 176
 Park C.-G., Ratra B., 2018a, *ApJ*, 868, 83
 Park C.-G., Ratra B., 2018b, *ApSS*, 364, 82
 Park C.-G., Ratra B., 2019, *ApJ*, 882, 158
 Park C.-G., Ratra B., 2018d, *ApSS*, 364, 134
 Park C.-G., Ratra B., 2020, *Phys.Rev. D*, 101, 083508
 Pavlov A., Westmoreland S., Saaïdi K, Ratra B., 2013, *Phys. Rev. D*, 88, 123513
 Peebles P.J.E., 1984, *ApJ*, 284, 439
 Peebles P.J.E., Ratra B., 1988, *ApJ*, 325, L17
 Planck Collaboration, 2018, preprint, (arXiv:1807.06209)
 Rameez M., Sarkar S., 2019, preprint, (arXiv: 1911.06456)
 Rana A., Jain D., Mahajan S., Mukherjee A., 2017, *JCAP*, 1703, 028
 Ratra B., Peebles P.J.E., 1988, *Phys. Rev. D*, 37, 3406
 Riess A. G., et al., 2016, *ApJ*, 826, 56
 Rigault M. et al., 2015, *ApJ*, 802, 20
 Risaliti G., Lusso E., 2015, *ApJ*, 815, 33
 Risaliti G., Lusso E., 2019, *Nat. Astron.*, 3, 272
 Ruan C.-Z., Melia F., Chen Y., Zhang T.-J., 2019, *ApJ*, 881, 137
 Ryan J., Chen Y., Ratra B., 2019, *MNRAS*, 488, 3844
 Ryan J., Doshi S., Ratra B., 2018, *MNRAS*, 480, 759
 Samushia L., Chen G., Ratra B., 2007, Preprint, (arXiv:0706.1963)
 Samushia L., Dev A., Jain D., Ratra B., 2010, *Physics Letters B*, 693, 509
 Samushia L., Ratra B., 2010, *ApJ*, 714, 1347
 Sangwan A., Tripathi A., Jassal H. K., 2018, preprint, (arXiv:1804.09350)
 SchÅúneberg N., Lesgourgues J., Hooper D. C., 2019, *JCAP*, 1910, 029
 Scolnic D. et al., 2018, *ApJ*, 859, 101
 Siegel E. et al., 2005, *MNRAS*, 356, 1117
 Singh A., Sangwan A., Jassal H. K., 2019, *JCAP*, 1904, 047
 Solà J., Gómez-Valent A., Pérez J. d. C., 2017, *Mod. Phys. Lett.*, A32, 1750054
 Solà Peracaula J., Pérez J. d. C., Gómez-Valent A., 2018, *MNRAS*, 478, 4357
 Solà Peracaula J., Gómez-Valent A., Pérez J. d. C., 2019, *Phys. Dark Univ.*, 25, 100311
 Steffen A. T., Strateva I., Brandt W. N. et al., 2006, *AJ*, 131, 2826

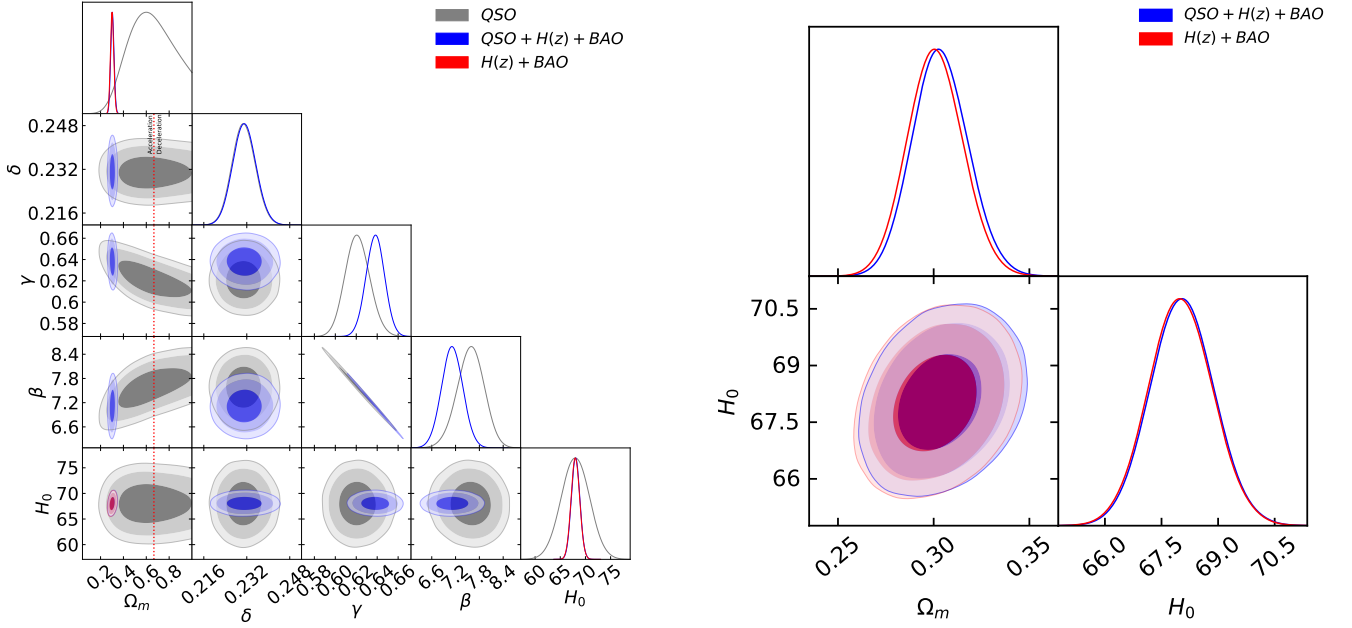


Figure 4. Flat Λ CDM model constraints from QSO (grey), $H(z)$ + BAO (red), and QSO + $H(z)$ + BAO (blue) data. Left panel shows 1, 2, and 3 σ confidence contours and one-dimensional likelihoods for all free parameters. The red dotted straight lines are zero acceleration lines, with currently accelerated cosmological expansion occurring to the left of the lines. Right panel shows magnified plots for only cosmological parameters Ω_{m0} and H_0 , without the QSO-only constraints. These plots are for the $H_0 = 68 \pm 2.8 \text{ km s}^{-1} \text{ Mpc}^{-1}$ prior.

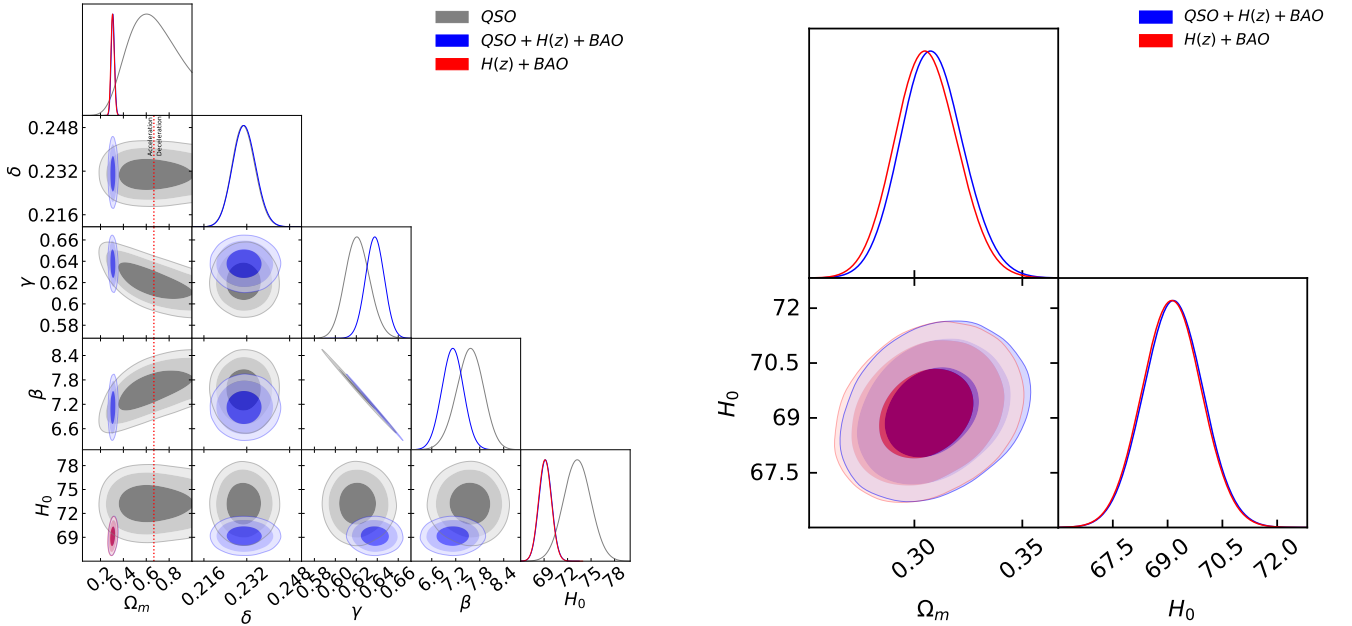


Figure 5. Flat Λ CDM model constraints from QSO (grey), $H(z)$ + BAO (red), and QSO + $H(z)$ + BAO (blue) data. Left panel shows 1, 2, and 3 σ confidence contours and one-dimensional likelihoods for all free parameters. The red dotted straight lines are zero acceleration lines, with currently accelerated cosmological expansion occurring to the left of the lines. Right panel shows magnified plots for only cosmological parameters Ω_{m0} and H_0 , without the QSO-only constraints. These plots are for the $H_0 = 73.24 \pm 1.74 \text{ km s}^{-1} \text{ Mpc}^{-1}$ prior.

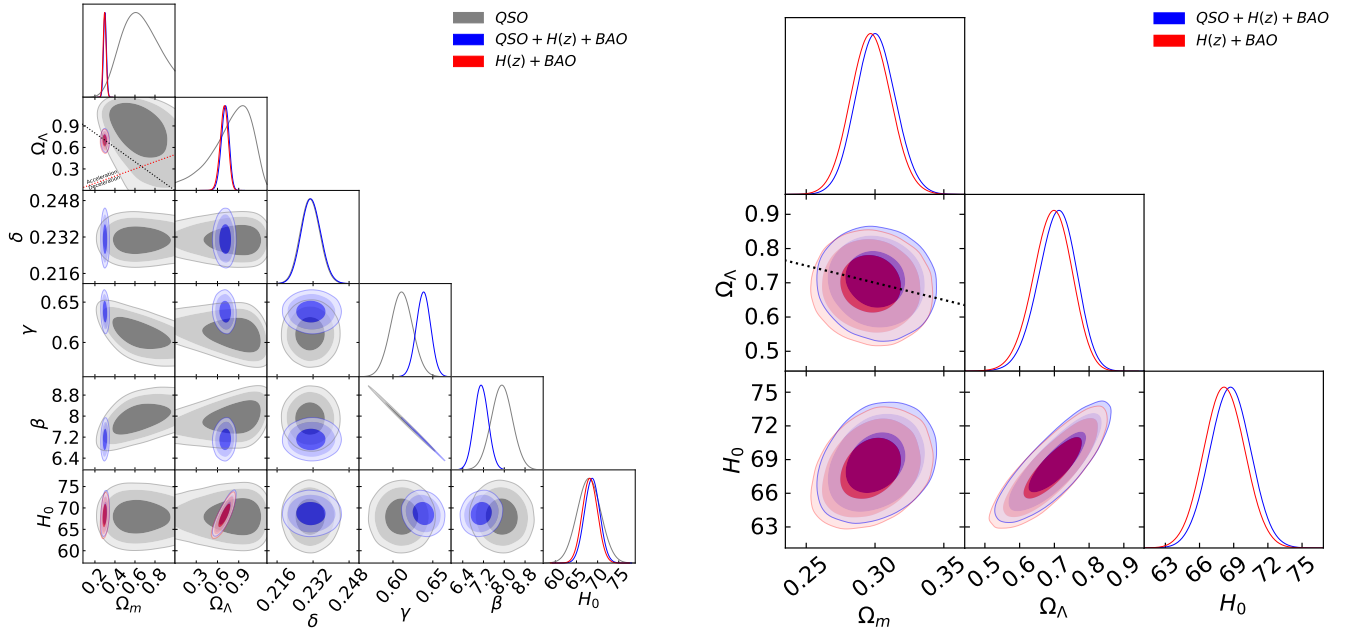


Figure 6. Non-flat Λ CDM model constraints from QSO (grey), $H(z)$ + BAO (red), and QSO + $H(z)$ + BAO (blue) data. Left panel shows 1, 2, and 3 σ confidence contours and one-dimensional likelihoods for all free parameters. The red dotted straight line in the $\Omega_\Lambda - \Omega_{m0}$ panel is the zero acceleration line with currently accelerated cosmological expansion occurring to the upper left of the line. Right panel shows magnified plots for cosmological parameters Ω_{m0} , Ω_Λ , and H_0 , without the QSO-only constraints. These plots are for the $H_0 = 68 \pm 2.8 \text{ km s}^{-1}\text{Mpc}^{-1}$ prior. The black dotted straight line in the $\Omega_\Lambda - \Omega_{m0}$ panels correspond to the flat Λ CDM model, with closed spatial geometry being to the upper right.

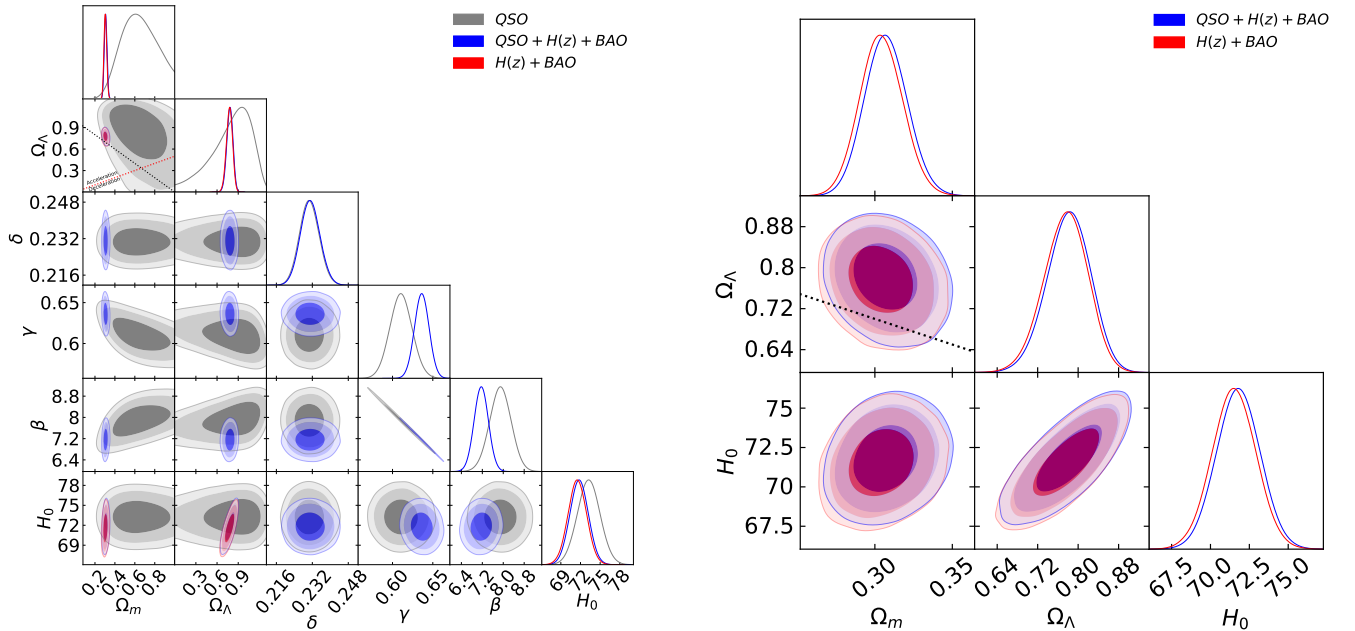


Figure 7. Non-flat Λ CDM model constraints from QSO (grey), $H(z)$ + BAO (red), and QSO + $H(z)$ + BAO (blue) data. The red dotted straight line in the $\Omega_\Lambda - \Omega_{m0}$ panel is the zero acceleration line with currently accelerated cosmological expansion occurring to the upper left of the line. Left panel shows 1, 2, and 3 σ confidence contours and one-dimensional likelihoods for all free parameters. Right panel shows magnified plots for only cosmological parameters Ω_{m0} , Ω_Λ , and H_0 , without the QSO-only constraints. These plots are for the $H_0 = 73.24 \pm 1.74 \text{ km s}^{-1}\text{Mpc}^{-1}$ prior. The black dotted straight line in the $\Omega_\Lambda - \Omega_{m0}$ panels correspond to the flat Λ CDM model, with closed spatial geometry being to the upper right.

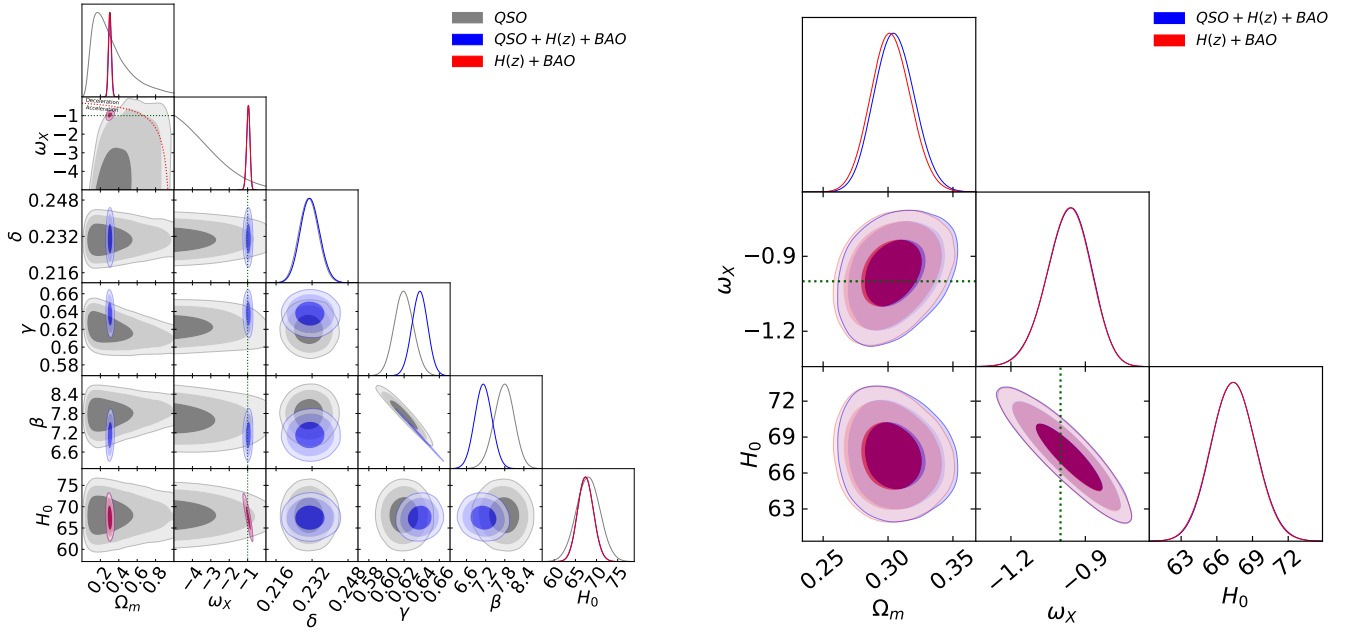


Figure 8. Flat XCDM parametrization constraints from QSO (grey), $H(z) + \text{BAO}$ (red), and QSO + $H(z) + \text{BAO}$ (blue) data. Left panel shows 1, 2, and 3 σ confidence contours and one-dimensional likelihoods for all free parameters. The red dotted curved line in the $\omega_X - \Omega_m$ panel is the zero acceleration line with currently accelerated cosmological expansion occurring below the line. Right panel shows magnified plots for only cosmological parameters Ω_m , ω_X , and H_0 , without the QSO-only constraints. These plots are for the $H_0 = 68 \pm 2.8 \text{ km s}^{-1} \text{ Mpc}^{-1}$ prior. The green dotted straight lines represent $\omega_X = -1$.

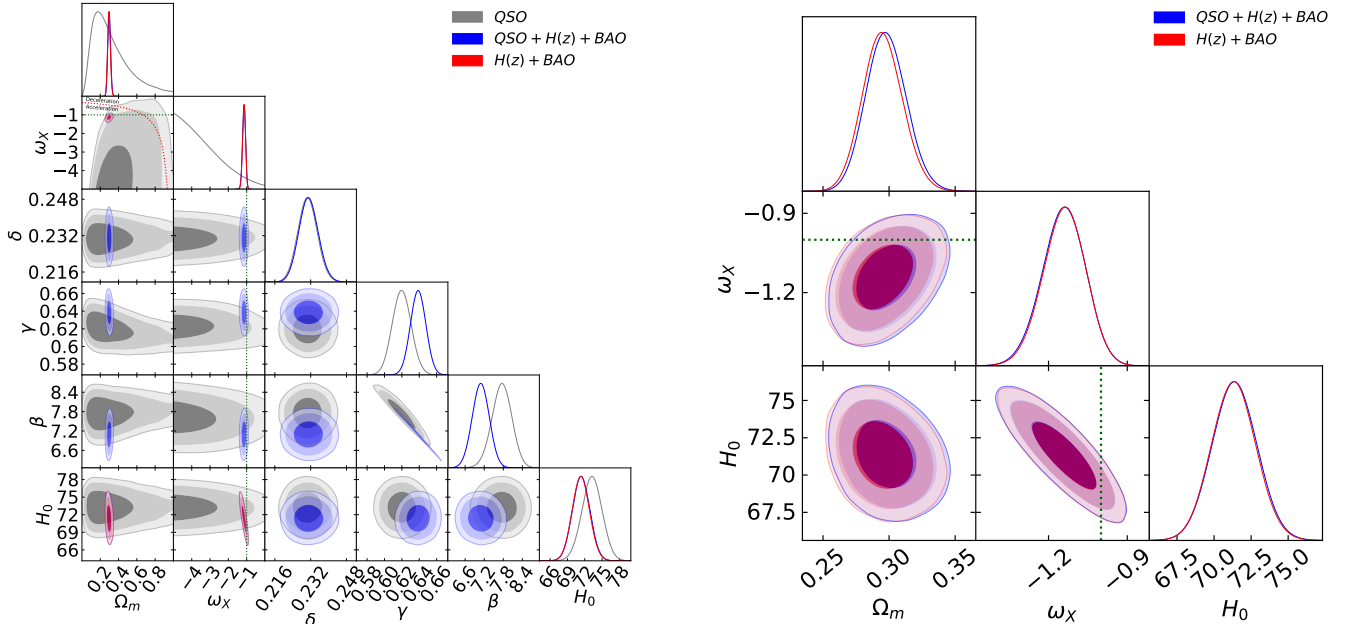


Figure 9. Flat XCDM parametrization constraints from QSO (grey), $H(z) + \text{BAO}$ (red), and QSO + $H(z) + \text{BAO}$ (blue) data. Left panel shows 1, 2, and 3 σ confidence contours and one-dimensional likelihoods for all free parameters. The red dotted curved line in the $\omega_X - \Omega_m$ panel is the zero acceleration line with currently accelerated cosmological expansion occurring below the line. Right panel shows magnified plots for only cosmological parameters Ω_m , ω_X , and H_0 , without the QSO-only constraints. These plots are for the $H_0 = 73.24 \pm 1.74 \text{ km s}^{-1} \text{ Mpc}^{-1}$ prior. The green dotted straight lines represent $\omega_X = -1$.

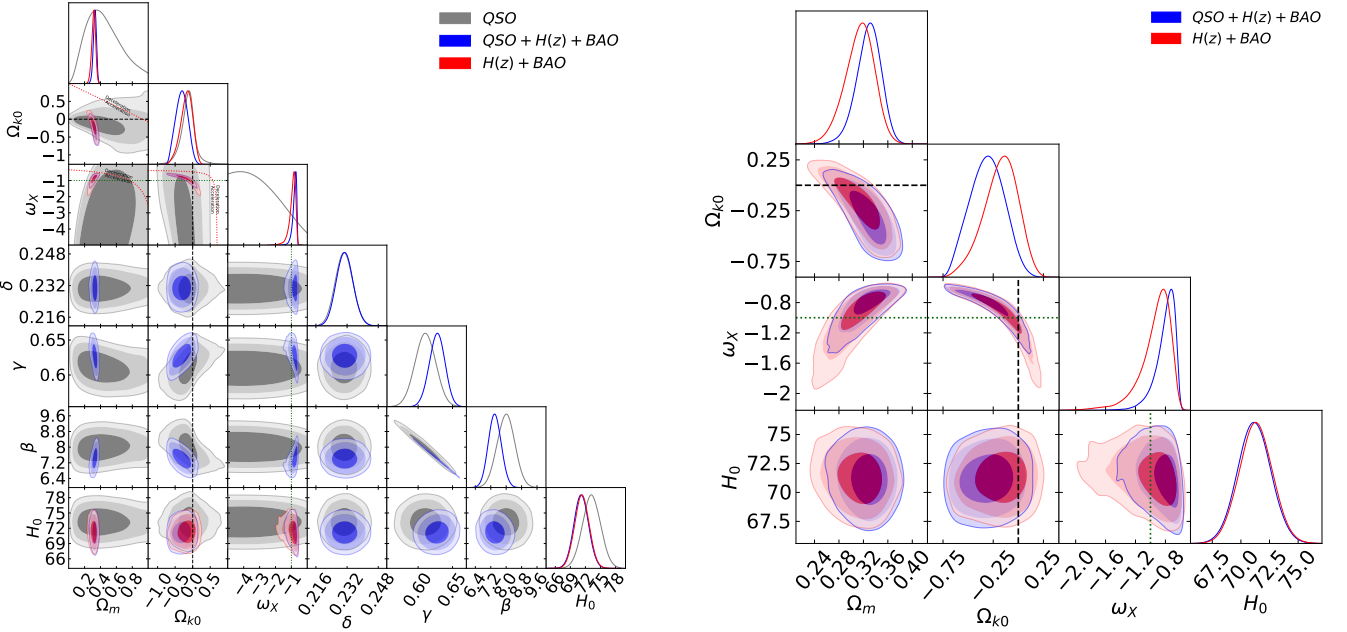


Figure 11. Non-flat XCDM parametrization constraints from QSO (grey), $H(z) + \text{BAO}$ (red), and $\text{QSO} + H(z) + \text{BAO}$ (blue) data. Left panel shows 1, 2, and 3 σ confidence contours and one-dimensional likelihoods for all free parameters. The red dotted curved lines in the $\omega_x - \Omega_{k0}$, $\omega_x - \Omega_m$, and $\omega_x - \Omega_{k0}$ panels are the zero acceleration lines with currently accelerated cosmological expansion occurring below the lines. Each of the three lines are computed with the third parameter set to the QSO data only best-fit value of Table 4. Right panel shows magnified plots for only cosmological parameters Ω_m , Ω_{k0} , ω_x , and H_0 , without the QSO-only constraints. These plots are for the $H_0 = 73.24 \pm 1.74 \text{ km s}^{-1} \text{ Mpc}^{-1}$ prior. The black dashed straight lines and the green dotted straight lines are $\Omega_{k0} = 0$ and $\omega_x = -1$ lines.

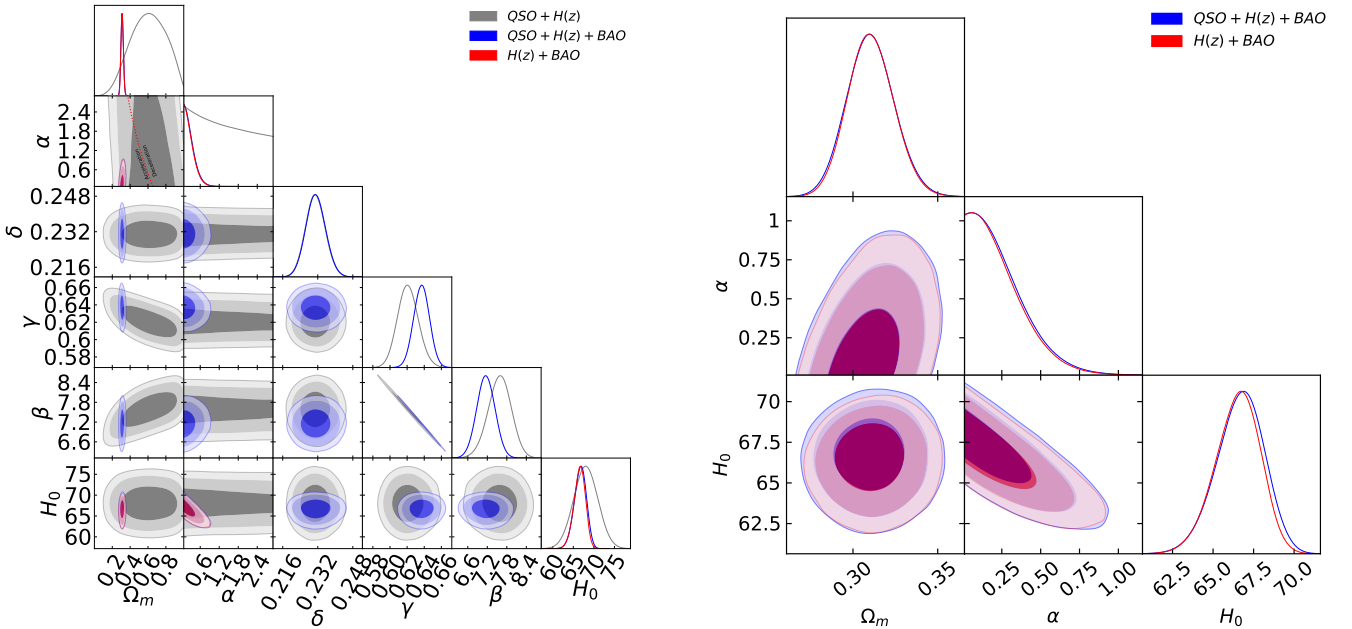


Figure 12. Flat ϕCDM model constraints from QSO (grey), $H(z) + \text{BAO}$ (red), and $\text{QSO} + H(z) + \text{BAO}$ (blue) data. Left panel shows 1, 2, and 3 σ confidence contours and one-dimensional likelihoods for all free parameters. The red dotted curved line in the $\alpha - \Omega_m$ panel is the zero acceleration line, with currently accelerated cosmological expansion occurring to the left of the line. Right panel shows magnified plots for only cosmological parameters Ω_m , α , and H_0 , without the QSO-only constraints. These plots are for the $H_0 = 68 \pm 2.8 \text{ km s}^{-1} \text{ Mpc}^{-1}$ prior.

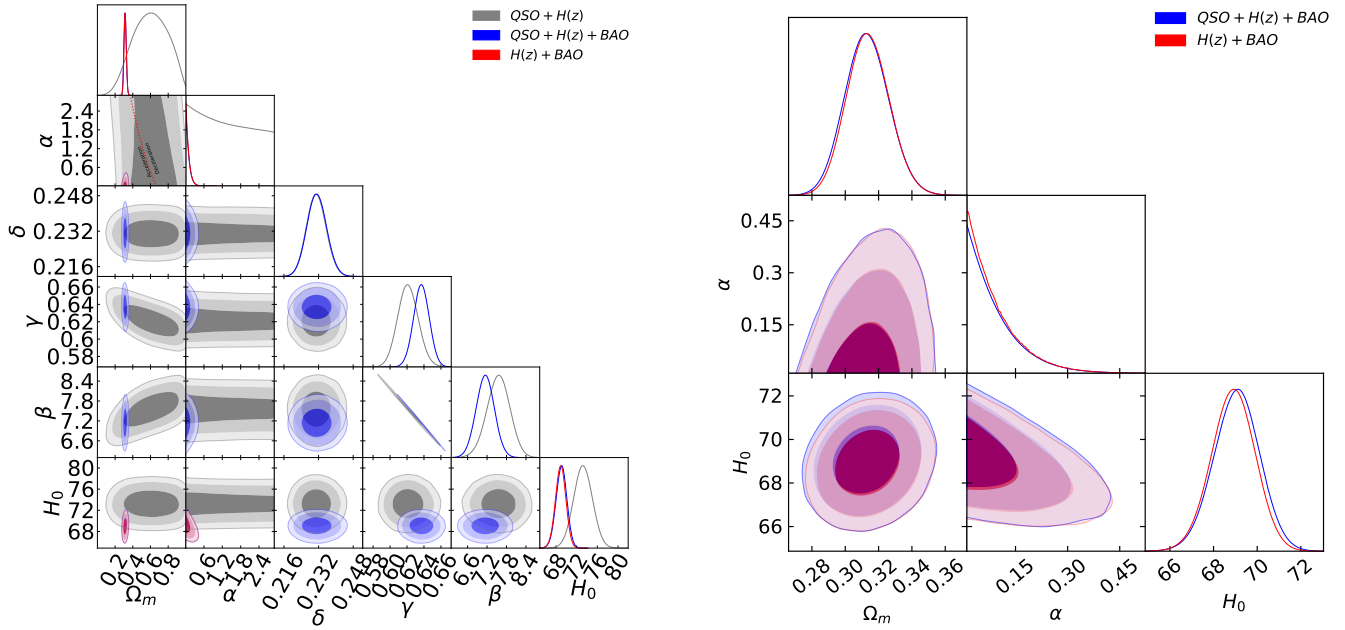


Figure 13. Flat ϕ CDM model constraints from QSO (grey), $H(z)$ + BAO (red), and QSO + $H(z)$ + BAO (blue) data. Left panel shows 1, 2, and 3σ confidence contours and one-dimensional likelihoods for all free parameters. The red dotted curved line in the $\alpha - \Omega_{m0}$ panel is the zero acceleration line, with currently accelerated cosmological expansion occurring to the left of the line. Right panel shows magnified plots for only cosmological parameters Ω_{m0} , α , and H_0 , without the QSO-only constraints. These plots are for the $H_0 = 73.24 \pm 1.74$ km s $^{-1}$ Mpc $^{-1}$ prior.

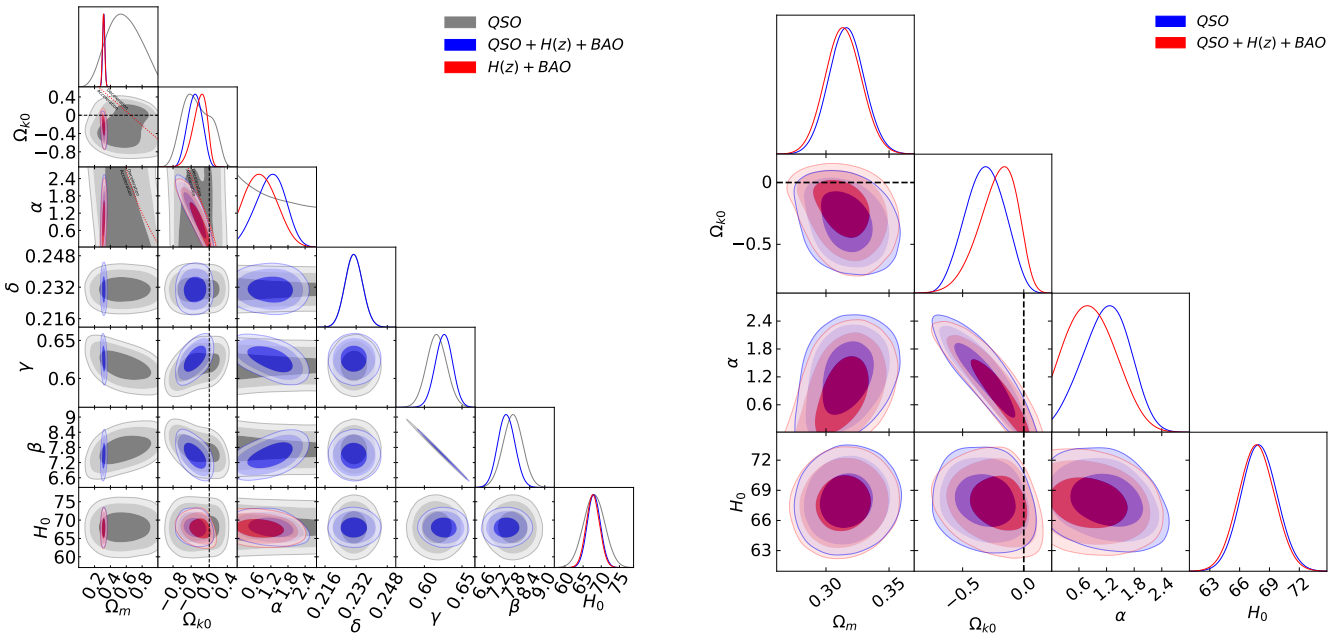


Figure 14. Non-flat ϕ CDM model constraints from QSO (grey), $H(z)$ + BAO (red), and QSO + $H(z)$ + BAO (blue) data. Left panel shows 1, 2, and 3σ confidence contours and one-dimensional likelihoods for all free parameters. The red dotted curved lines in the $\Omega_{k0} - \Omega_{m0}$, $\alpha - \Omega_{m0}$, and $\alpha - \Omega_{k0}$ panels are the zero acceleration lines with currently accelerated cosmological expansion occurring below the lines. Each of the three lines are computed with the third parameter set to the QSO data only best-fit value of Table 3. Right panel shows magnified plots for only cosmological parameters Ω_{m0} , Ω_{k0} , α , and H_0 , without the QSO-only constraints. These plots are for the $H_0 = 68 \pm 2.8$ km s $^{-1}$ Mpc $^{-1}$ prior. The black dashed straight lines are $\Omega_{k0} = 0$ lines.

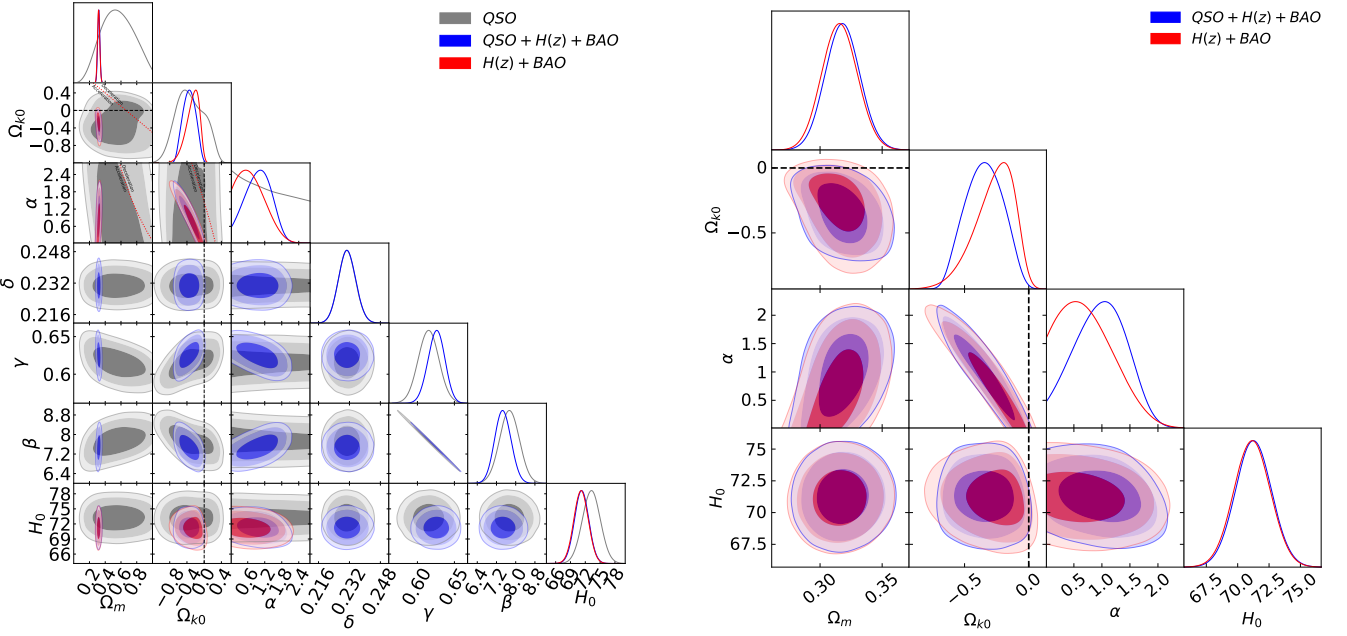


Figure 15. Non-Flat ϕ CDM model constraints from QSO (grey), $H(z)$ + BAO (red), and QSO + $H(z)$ + BAO (blue) data. Left panel shows 1, 2, and 3 σ confidence contours and one-dimensional likelihoods for all free parameters. The red dotted curved lines in the $\omega_{K0} - \Omega_{m0}$, $\alpha - \Omega_{m0}$, and $\alpha - \Omega_{K0}$ panels are the zero acceleration lines with currently accelerated cosmological expansion occurring below the lines. Each of the three lines are computed with the third parameter set to the QSO data only best-fit value of Table 4. Right panel shows magnified plots for only cosmological parameters Ω_{m0} , Ω_{k0} , α , and H_0 , without the QSO-only constraints. These plots are for the $H_0 = 73.24 \pm 1.74 \text{ km s}^{-1} \text{ Mpc}^{-1}$ prior. The black dashed straight lines are $\Omega_{k0} = 0$ lines.